

A new tool for clustered survival data and multiple treatments: Estimation of treatment effect heterogeneity and variable selection

Liangyuan Hu¹

Abstract

A new tool, riAFT-BART, was recently developed to draw causal inferences about population treatment effect on patient survival from clustered and censored survival data while accounting for the multilevel data structure. The practical utility of this tool goes beyond the estimation of population average treatment effect. In this work, we exposit how riAFT-BART can be used to solve two important statistical questions with clustered survival data: estimating the treatment effect heterogeneity and variable selection. Leveraging the likelihood-based machine learning, we describe a way in which we can draw posterior samples of the individual survival treatment effect from riAFT-BART model runs, and use the drawn posterior samples to perform an exploratory treatment effect heterogeneity analysis to identify subpopulations who may experience differential treatment effects than population average effects. There is sparse literature on methods for variable selection among clustered and censored survival data, particularly ones using flexible modeling techniques. We propose a permutation based approach using the predictor's variable inclusion proportion supplied by the riAFT-BART model for variable selection. To address the missing data issue frequently encountered in health databases, we propose a strategy to combine bootstrap imputation and riAFT-BART for variable selection among incomplete clustered survival data. We conduct an expansive simulation study to examine the practical operating characteristics of our proposed methods, and provide empirical evidence that our proposed methods perform better than several existing methods across a wide range of data scenarios. Finally, we demonstrate the methods via a case study of predictors for in-hospital mortality among severe COVID-19 patients and estimating the heterogeneous treatment effects of three COVID-specific medications. The methods developed in this work are readily available in the R package riAFTBART.

Keywords

Missing at random, Variable importance, Tree ensemble, Bootstrap imputation, Variable selection

1 Introduction

Large-scale healthcare datasets garnered from multiple facilities are increasingly available, offering fertile ground for innovative investigation into emerging medical research questions. The inherent hierarchical data structure, in conjunction with the censored survival outcome, which is of strong clinical interest, poses considerable challenges for statistical analysis. Hu et al.¹ recently developed a flexible approach, riAFT-BART to estimate the population average treatment effect on patient survival, while accounting for the clustering structure of the observations. The method riAFT-BART stands for random-intercept accelerated failure time model with Bayesian additive regression trees (BART).² The utility of this new tool, which leverages Bayesian machine learning, goes beyond the estimation of population average treatment effect. In this article, we exposit how riAFT-BART can be used to solve two important statistical questions with clustered survival data: estimating the treatment effect heterogeneity and variable selection.

An immediate extension of the new tool, riAFT-BART, beyond the population average treatment effect is the estimation of heterogeneous treatment effect. Prior work³ has shown that compared to algorithm-based machine learning, leveraging the likelihood-based machine learning technique BART can provide more accurate estimation of the individual survival treatment effect, which in turn can be used to assess the treatment effect heterogeneity. To the best of our knowledge, no work has yet discussed how BART can be used to estimate the heterogeneous effect of multiple treatments on patient survival using clustered survival observations.

¹Department of Biostatistics and Epidemiology, Rutgers University School of Public Health, USA

Corresponding author:

Liangyuan Hu, Department of Biostatistics and Epidemiology, Rutgers University School of Public Health, 683 Hoes Lane West, Piscataway, NJ, USA 08854.

Email: liangyuan.hu@rutgers.edu

Another important utility of riAFT-BART is for variable selection with clustered survival data, on which there is sparse literature. Fan et al.⁴ proposed a family of variable selection methods for the gamma frailty model based on a nonconcave penalized likelihood approach using the Newton-Raphson method. Androulakis et al.⁵ extended the penalized Cox or Gamma frailty model to a class of frailty models and proposed a generalized form of the likelihood function to allow the use of different continuous distributions for the frailty term. Utazirubanda et al.⁶ proposed group LASSO with gamma-distributed frailty for variable selection in Cox regression. However, no corresponding software is available for these methods. Bender et al.⁷ proposed a piece-wise exponential additive mixed model (PEAMM) for clustered survival data, and Marra and Wood⁸ described a practical approach by which shrinkage penalties can be added to the smoothing parameters in PEAMM and variable selection can be performed by using restricted maximum likelihood estimation. Rondeau et al.⁹ proposed to conduct variable selection by maximizing the penalized likelihood using the Marquardt algorithm,¹⁰ which is a combination of the Newton-Raphson algorithm and the steepest descent algorithm. Ha et al.¹¹ proposed a penalized h-likelihood estimation approach for variable selection of fixed effects using semiparametric frailty models. These methods rely on parametric assumptions about the exact relationships between covariates and survival outcomes. Misspecifying the parametric forms of covariate-outcome relationships can reverberate through the variable selection procedure and yield unsatisfactory results.^{12,13}

Flexible machine learning modeling techniques can help relax the parametric assumptions and improve variable selection results. Ishwaran et al.¹⁴ derived the distribution of the minimal depth of a maximal subtree, which measures the predictiveness of a variable in a survival tree, and used it for high-dimensional variable selection using random survival forests. Lagani et al.¹⁵ proposed an algorithm based on the theory of Bayesian networks and the Markov blanket for variable selection suitable for high-dimensional and right-censored survival data. However, neither of these two machine learning based methods accommodates clustered survival observations.

In this work, we describe ways in which riAFT-BART can be used to (i) detect and estimate the treatment effect heterogeneity, and to (ii) select important predictors in the presence of missing data with clustered survival observations. The rest of the paper is organized as follows. Section 2 describes the use of riAFT-BART for estimating individual survival treatment effects and exploring subgroups who may experience enhanced or reduced treatment effect than population average treatment effect. Section 3 proposes a variable selection method using riAFT-BART when covariates are subject to missing data. In Section 4, we conduct an expansive simulation to assess the practical operating characteristics of riAFT-BART in estimating treatment effect heterogeneity and performing variable selection. Section 5 illustrates the methods using a COVID-19 dataset drawn from the Mount Sinai Medical Center, and Section 6 provides a discussion.

2 Estimation of Treatment Effect Heterogeneity

2.1 Notation

We maintain notation used in Hu et al.¹ Consider a nonexperimental study with K clusters, each having treated n_k individuals, indexed by $i = 1, \dots, n_k, k = 1, \dots, K$. There are J possible treatment options, denoted by $A \in \mathcal{A} = \{a_1, \dots, a_J\}$. Denote pre-treatment measured, L -dimensional covariates by $\mathbf{X}_{ik} = \{X_{ik1}, \dots, X_{ikL}\}$ for each individual i in cluster k , whose failure time T_{ik} may be right censored at C_{ik} . The observed outcome consists of $Y_{ik} = \min(T_{ik}, C_{ik})$ and the censoring indicator $\Delta_{ik} = I(T_{ik} < C_{ik})$. Let V_k be the cluster indicators. Proceeding with the counterfactual framework, the counterfactual failure time under treatment a_j for individual i in cluster k is defined as $T_{ik}(a_j), \forall a_j \in \mathcal{A}$, and the counterfactual censoring time under treatment a_j is defined as $C_{ik}(a_j)$. Throughout, we maintained the standard assumptions:^{1,3,16–18} consistency, weak unconfoundedness, positivity and covariate-dependent censoring, for drawing causal inference with observational clustered survival data. Detailed assumptions and implications of assumptions can be found in Hu et al.¹

2.2 Method

Hu et al.¹ adapted BART into a random-intercept accelerated failure time model,

$$\begin{aligned} \log T_{ik} &= f(A_{ik}, \mathbf{X}_{ik}) + b_k + \epsilon_{ik}, \\ b_k &\overset{i.i.d.}{\sim} N(0, \alpha_k \tau^2), \quad \epsilon_{ik} \overset{i.i.d.}{\sim} N(0, \sigma^2), \quad b_k \perp \epsilon_{ik}, \end{aligned} \quad (1)$$

where $f(A_{ik}, \mathbf{X}_{ik})$ is an unspecified function relating treatment assignment A_{ik} and pretreatment confounders \mathbf{X}_{ik} to survival times T_{ik} , b_k 's are the random intercepts capturing cluster-specific main effects, and ϵ_{ik} is the residual term. The unknown function f is flexibly modeled by BART via a sum of shallow trees.^{19,20} A mean-zero normal distribution and independence are assumed for b_k and ϵ_{ik} . A redundant parameter α_k was used for the variance of b_k as a parameter expansion technique²¹ to improve computational performance. Regularizing priors are placed on the tree parameters to keep the impact of each individual tree on the overall fit small and thus prevent overfitting.² Sensible priors are used for parameters σ^2 , τ^2 and α_k .^{1,22} To deal with right censoring, data augmentation is used. That is, the unobserved survival times are imputed from a truncated normal distribution in each Gibbs iteration. A Metropolis within Gibbs procedure¹ was proposed to draw posterior inferences about the population average treatment effect on patient survival, which is defined as

$$\theta_{a_j, a_{j'}} = \frac{1}{N} \sum_{k=1}^K \sum_{i=1}^{n_k} E[T_{ik}(a_j) - T_{ik}(a_{j'}) | \mathbf{X}_{ik} = \mathbf{x}_{ik}, V_k = v_k], \quad \forall a_j, a_{j'} \in \mathcal{A}.$$

Via outcome modeling, the pairwise population average treatment effect between a_j and $a_{j'}$ can be estimated as

$$\hat{\theta}_{a_j, a_{j'}} = \frac{1}{D} \sum_{d=1}^D \frac{1}{n_k K} \sum_{k=1}^K \sum_{i=1}^{n_k} \left\{ \tilde{f}^d(a_j, \mathbf{x}_{ik}) - \tilde{f}^d(a_{j'}, \mathbf{x}_{ik}) \right\}, \quad (2)$$

where \tilde{f}^d is the d th draw from the posterior distribution of f . Inferences can be obtained based on the D posterior average treatment effects, $(1/n_k K) \sum_{k=1}^K \sum_{i=1}^{n_k} \left\{ \tilde{f}^d(a_j, \mathbf{x}_{ik}) - \tilde{f}^d(a_{j'}, \mathbf{x}_{ik}) \right\}$, $d = 1, \dots, D$.

Turning to the estimation of treatment effect heterogeneity. We first define the *individual survival treatment effect* (ISTE) for individual i in cluster k as

$$\zeta_{a_j, a_{j'}}(\mathbf{x}_{ik}) = E[\log T_{ik}(a_j) - \log T_{ik}(a_{j'}) | \mathbf{x}_{ik}, v_k], \quad (3)$$

which will be used as the building block for estimating the heterogeneous treatment effect. From the fitted Model (1), we can estimate $\zeta_{a_j, a_{j'}}(\mathbf{x}_{ik})$ as

$$\hat{\zeta}_{a_j, a_{j'}}(\mathbf{x}_{ik}) = \tilde{f}(a_j, \mathbf{x}_{ik}) - \tilde{f}(a_{j'}, \mathbf{x}_{ik}),$$

where \tilde{f} is the mean of D draws from the posterior predictive distribution of f . The ISTE estimates $\{\hat{\zeta}_{a_j, a_{j'}}(\mathbf{x}_{ik}), i = 1, \dots, n_k, k = 1, \dots, K\}$ can then be used to explore the degree of treatment effect heterogeneity. By the “virtual twins” approach,²³ the $\{\hat{\zeta}_{a_j, a_{j'}}(\mathbf{x}_{ik})\}$ would be regressed on the predictors via a tree diagram to identify the predictor subspaces that explain away differences in $\{\hat{\zeta}(\mathbf{x}_{ik})\}$. In a similar spirit, the “fit-the-fit” strategy has been used to identify possible subgroups defined by combination rules of covariates that have differential treatment effects.^{3,24,25} Mathematically, we wish to find a covariate subspace $\mathcal{S}_{a_j, a_{j'}} = \{S_{a_j, a_{j'}}^1, S_{a_j, a_{j'}}^2, \dots, S_{a_j, a_{j'}}^H\}$, where $h \in \{1, \dots, H\}$ is the number of combination rules of covariates, such that the average treatment effects across individuals in this region are considerably different than the population average treatment effect. Denote the measure of subgroup treatment effect between a_j and $a_{j'}$ as $\mathcal{M}(\mathcal{S}_{a_j, a_{j'}}) = \{M(S_{a_j, a_{j'}}^1), \dots, M(S_{a_j, a_{j'}}^H)\}$, and

$$M(S_{a_j, a_{j'}}^h) = E[\zeta_{a_j, a_{j'}}(\mathbf{x}_{ik}) | \mathbf{x}_{ik} \in S_{a_j, a_{j'}}^h]. \quad (4)$$

We adopt the “fit-the-fit” strategy to estimate $\mathcal{S}_{a_j, a_{j'}}$ and $\mathcal{M}(\mathcal{S}_{a_j, a_{j'}})$. The algorithm proceeds with the following steps:

1. Add each candidate predictor separately to the random forests model²⁶ using $\{\hat{\zeta}_{a_j, a_{j'}}(\mathbf{x}_{ik})\}$ as the outcome, and record the model fit measured by R^2 ; include the predictor corresponding to the largest R^2 in the model;
2. Add each of the remaining candidate predictors separately to the previous step’s model and retain the predictor corresponding to the largest R^2 improvement;
3. Repeat step 2 until the percent improvement in R^2 is less than 1%.

Different from prior work, we use random forests instead of a single tree to regress the ISTE estimates on predictors for improved modeling accuracy and stability. To interpret the tree ensembles in the final random forests model yielded in Step 3, we apply the `inTrees` algorithms²⁷ to translate the composite rules into a simple rule model. The `inTrees` algorithms extract, measure and rank rules, prune redundant rules, detect frequent variable interactions, and summarize rules into a simple tree diagram model that can be used for predicting new data. The branch decision rules in the final tree diagram model sending individuals to the terminal nodes suggest the predictor subspace $\hat{\mathcal{S}}_{a_j, a_{j'}}^h$; and subgroup treatment effects that are substantially different from the population effect $\theta_{a_j, a_{j'}}$ can then be estimated by averaging the ISTE estimates among individuals falling into each of terminal nodes,

$$\hat{M}(\hat{\mathcal{S}}_{a_j, a_{j'}}^h) = \frac{1}{|\hat{\mathcal{S}}_{a_j, a_{j'}}^h|} \sum_{i, k: \mathbf{x}_{ik} \in \hat{\mathcal{S}}_{a_j, a_{j'}}^h} \hat{\zeta}_{a_j, a_{j'}}(\mathbf{x}_{ik}),$$

where $|\hat{\mathcal{S}}_{a_j, a_{j'}}^h|$ is the size of $\hat{\mathcal{S}}_{a_j, a_{j'}}^h$.

3 Variable Selection

Variable selection has been a longstanding statistical problem and studied from both the classical and Bayesian perspective. In the field of causal inference, variable selection methods can aid in confounder selection.²⁸ Variable selection methods are largely based on parametric models, in which the exact relationships between the response and predictor variables need to be explicitly specified. However, incorrectly specifying the parametric models may produce unsatisfactory variable selection results.^{12,13,29} For example, noise variables may be selected and important variables ignored. Flexible machine learning models can better represent functional forms of arbitrary complexity, thus mitigate parametric assumptions and attendant errors in variable selection. We develop a way in which the new tool `riAFT-BART` can be used for variable selection among clustered survival data. Notation defined in Section 2.1 is largely retained with the exception of treatment assignment A_{ik} , as the focus now is variable selection.

3.1 Random-intercept accelerated failure time model with Bayesian additive regression trees

We propose a permutation-based approach for variable selection. Following prior work,^{12,13,29} we use the variable inclusion proportion (VIP) of each predictor variable as the foundation to determine how important a predictor variable is. The VIP score is supplied by the BART model, and is computed as the proportion of times each predictor is chosen as a splitting rule divided by the total number of splitting rules appearing in the model.³⁰ We note that in the riAFT-BART model (1), the predictor variables \mathbf{X}_{ik} , along with treatment assignment A_{ik} , is included in the unknown function $f(A_{ik}, \mathbf{X}_{ik})$, which is being modeled by BART. Thus, in each iteration of the riAFT-BART sampling algorithm,¹ we can extract the VIP for each predictor variable in the step where a BART model is fit to regress $\log y_{ik}^{cent,c} - b_k$ on $\{A_{ik}, \mathbf{X}_{ik}\}$, where $y_{ik}^{cent,c}$ denotes the centered and complete survival time. Note that right censoring is addressed via data augmentation. Detailed riAFT-BART sampling algorithm appears in Web Section 1. For each predictor variable X_l , $l \in \{1, \dots, L\}$ (we suppress subscripts i and k for brevity of notation), we compute its VIP by averaging the VIP scores across D posterior draws,¹³ $VIP_{x_l} = \frac{1}{D} \sum_{d=1}^D \widehat{VIP}_{x_l}^d$, $d = 1, \dots, D$, where $\widehat{VIP}_{x_l}^d$ is the d th draw from the posterior distribution of the VIP for X_l . In our simulation (Section 4), we set $D = 4500$ with the first 1000 discarded as burn-in. Trace plot was used to check the convergence of the posterior distribution of the VIP for X_l .

Building on prior literature,^{13,31} we propose a non-parametric and permutation-based approach for variable selection, by which we first permute the event times together with the censoring indicators and then establish the thresholds for variable selection using the VIP from observed data and the permuted data. Specifically, we first create P permutations of the vectors of observed survival times and event indicators $(\mathbf{y}, \Delta) = \{Y_{11}, \Delta_{11}, \dots, Y_{n_k K}, \Delta_{n_k K}\} : (\mathbf{y}_1^*, \Delta_1^*), (\mathbf{y}_2^*, \Delta_2^*) \dots, (\mathbf{y}_P^*, \Delta_P^*)$. Then for each of the permuted outcome vectors $(\mathbf{y}_p^*, \Delta_p^*)$, we fit an riAFT-BART model with $(\mathbf{y}_p^*, \Delta_p^*)$ as the response and the original $\{\mathbf{X}_{ik}\}$ as predictor variables and V_k as cluster indicator. This permutation strategy removes any dependency between the predictors $\{\mathbf{X}_{ik}\}$ and the outcomes $\{(Y_{ik}, \Delta_{ik})\}$ while keeping possible dependencies among the predictor variables. From the riAFT-BART run using each permuted outcome vector $(\mathbf{y}_p^*, \Delta_p^*)$, we retain the VIP for each predictor variable. We use $VIP_{x_l, p}^*$ to denote the VIP score from riAFT-BART for predictor X_l from the p th permuted outcomes, and use the notation $VIP_{\mathbf{X}, p}^*$ for the vector of all L VIPs from the p th permuted outcomes, $(VIP_{x_1, p}^*, \dots, VIP_{x_L, p}^*)$. As suggested by Bleich et al.¹³, we use the VIPs across all P permutations $VIP_{\mathbf{X}, 1}^*, \dots, VIP_{\mathbf{X}, P}^*$ as the “null” distribution for the VIPs from the unpermuted outcomes (\mathbf{y}, Δ) , $VIP_{x_1}, \dots, VIP_{x_L}$. The permutation null distribution will be used to determine which variables should be selected or deemed as important. We adopt the “local” threshold strategy, which has been shown in several works^{12,13,29,32,33} to have better performance than more stringent strategies such as “global max” for large-scale healthcare data in which the ratio of sample size and number of predictors is relatively large. More stringent strategies compare the VIP of a predictor VIP_{x_l} to the permutation distribution across all predictor variables $VIP_{\mathbf{X}, 1}^*, \dots, VIP_{\mathbf{X}, P}^*$. By contrast, a local threshold compares VIP_{x_l} with its own permutation null distribution $VIP_{x_l, 1}^*, \dots, VIP_{x_l, P}^*$. Specifically, we only select predictor X_l if VIP_{x_l} is greater than the $1 - \alpha$ quantile of the permutation distribution $VIP_{x_l, 1}^*, \dots, VIP_{x_l, P}^*$. Following prior work,^{12,29} we set $\alpha = 0.05$ in our simulation and case study, because this threshold value has been shown to yield good variable selection results with a balance between selecting useful and selecting noise predictors.

3.2 Comparison methods

3.2.1 Piece-wise Exponential Additive Mixed Model For a PEAMM,⁷ the hazard rate at time t for individual i in cluster k with covariates \mathbf{X}_{ik} and cluster indicator V_k is given by

$$\lambda(t | \mathbf{X}_{ik}, V_k) = \exp \left\{ g_0(t_q) + \sum_{m=1}^M g_m(\mathbf{x}_{ik, m}) + b_k \right\} \forall t \in (\kappa_{q-1}, \kappa_q), \quad (5)$$

where $g_0(t_q)$ represents the log-baseline hazard rate, $g_m(\mathbf{x}_{ik, m})$ is the basis functions of natural cubic splines associated with the covariates \mathbf{x}_{ik} , b_k is the random intercept term capturing the cluster-specific effect, and κ_{q-1} and κ_q are the start and stop times of the censored survival dataset represented in the (start, stop] counting process form. For variable selection using PEAMM, following the practical approach by Marra and Wood et al.,⁸ a shrinkage penalty term can be added to each basis term $g_m(\mathbf{x}_{ik, m})$ of model (5):

$$\lambda(t | \mathbf{X}_{ik}, V_k) = \exp \left\{ g_0(t_q) + \sum_{m=1}^M \left(g_m(\mathbf{x}_{ik, m}) + \int g'_m(\mathbf{x}_{ik, m})^2 d\mathbf{x}_{ik, m} \right) + b_k \right\} \forall t \in (\kappa_{q-1}, \kappa_q),$$

so that when the whole spline basis terms for a predictor x_{ikl} are shrunk to zero, the variable x_{ikl} will be selected out of the model. The shrinkage penalties, along with all other model coefficients, can be estimated using restricted maximum likelihood estimation.

3.2.2 Frailty Models by Regularization Methods Given the common unobserved frailty u_k for cluster k , the conditional hazard function at time t for individual i in cluster k is

$$\lambda(t | \mathbf{X}_{ik}, V_k) = u_k \lambda_0(t) \exp(\mathbf{x}_{ik}^T \boldsymbol{\beta}) \quad (6)$$

where $\lambda_0(t)$ is an unspecified baseline hazard function and $\boldsymbol{\beta} = (\beta_1, \beta_2, \dots, \beta_L)^T$ is a vector of regression parameters for \mathbf{x}_{ik} . The common unobserved frailty u_k is assumed to follow a gamma distribution because of its mathematical convenience.

Rondeau et al.⁹ proposed to conduct variable selection by maximizing the penalized likelihood,

$$l(\lambda(t | \mathbf{X}_{ik}, V_k)) - \alpha \int_0^\infty \lambda_0''(t) dt,$$

where $l(\lambda(t | \mathbf{X}_{ik}, V_k))$ is the full marginal log-likelihood for the frailty model (6) and α is the smoothing parameter which controls the trade-off between the data fit and the smoothness of the baseline hazard function. The regression parameters can be estimated by the robust Marquardt algorithm¹⁰ – a combination of the Newton Raphson algorithm and the steepest descent algorithm. Do Ha et al.¹¹ instead proposed to perform variable selection by maximizing the penalized profile h-likelihood,

$$l^*(\lambda(t | \mathbf{X}_{ik}, V_k)) - \sum_{l=1}^L B_\gamma(|\beta_l|),$$

where $l^*(\lambda(t | \mathbf{X}_{ik}, V_k))$ is the profiled h-likelihood of the frailty model, $B_\gamma(|\beta_l|)$ is a penalty function that controls model complexity using the tuning parameter γ , with the optimal value determined by the Bayesian information criterion (BIC). Three penalty functions were considered for $B_\gamma(|\beta_l|)$: least absolute shrinkage and selection operator,³⁴ smoothly clipped absolute deviation,³⁵ and h-likelihood.³⁶

3.2.3 Backward stepwise selection We also implement a classical variable selection approach through a recursive procedure of backward stepwise selection based on statistical testing, as described in Wood et al.³⁷ The backward stepwise selection starts with a random-intercept Cox regression model³⁸ with all potential predictors and removes from the model the predictor that has the least impact on the fit determined by the α significance level. The forward selection process then checks whether removed variables should be added back into the model at $\alpha(1 - \epsilon)$ for ϵ small significance level. We use $\alpha = 0.05$ as suggested by Wood et al.³⁷

3.3 Variable selection with missing data

Large-scale healthcare data are susceptible to the missing data issue. Missing values in predictor variables pose challenges for variable selection. Long and Johnson³⁹ proposed a general resampling approach that combines bootstrap imputation and randomized lasso based variable selection procedure, and used simulations to demonstrate that this approach had better performance compared with several existing methods for variable selection in the presence of missing data. Recent work by Hu et al.¹² shows that combining bootstrap imputation with flexible machine learning based variable selection methods can substantially improve variable selection results over methods that rely on parametric modeling of the covariate-outcome relationship. In this work, we combine bootstrap imputation and variable selection, and compare each of the methods considered on the ability to select predictor variables that are truly associated with the outcome, or useful predictor variables, among *incomplete* clustered survival data. To stay consistent with the literature^{12,13,37} so that our methods and results can be compared with previous work in similar contexts, we use the following four performance metrics commonly used in the variable selection literature. A good method should have high values of precision, recall and F_1 , and low Type I error.

- (1) Precision = $TP / (TP + FP)$, where TP and FP are respectively the number of true positive and false positive selections. A true positive selection is when a useful predictor was selected; and a false positive selection is when a noise predictor was selected. The *precision* of a variable selection method is the proportion of truly useful predictors among all selected predictors.
- (2) Recall = $TP / (TP + FN)$, where FN is the number of false negative selections. A false negative selection is when a truly useful predictor was not selected. The *recall* of a variable selection method is the proportion of truly useful variables selected among all useful variables. This is sometimes referred to as the *power* in the literature.³⁷
- (3) $F_1 = 2 \text{ Precision} \times \text{Recall} / (\text{Precision} + \text{Recall})$. The F_1 score measures a method's ability to avoid selecting irrelevant predictors (precision) with its ability to identify the full set of useful predictors (recall).
- (4) Type I error. The *Type I error* measures the overall probability of a method incorrectly selecting the noise predictor – the mean of the probabilities that the method incorrectly selects each of the noise predictors.

Among incomplete data, we first conduct bootstrap imputation through two steps: (i) generate B bootstrap datasets of the original data; (ii) conduct a single imputation for each bootstrap dataset using an imputation method of choice. Following Hu et al.,¹² in our simulations and case study, we used $B = 100$ and performed standard imputation program using the R package `mice`. Variable selection via each of the methods considered was performed for all B bootstrap imputed datasets, and the final set of predictors were selected if they were selected in at least πB imputed datasets, where $\pi \in (0, 1)$ is a fraction threshold for selecting a predictor.

4 Simulation

4.1 Treatment effect heterogeneity

We carried out a contextualized simulation to evaluate the performance of our proposed method in estimating the heterogeneous treatment effect using observational data with clustered survival outcomes and multiple treatments. For methods comparison, we adapted the popularly used inverse probability weighting method into the setting of clustered and censored survival data to form two comparison methods: inverse probability of treatment weighting with the random-intercept Cox regression model (IPW-riCox) and doubly robust random-intercept additive hazards model (DR-riAH).⁴⁰ In addition, we considered the PEAMM⁷ – another outcome modeling based method flexible at capturing nonlinear relationships. Because not all methods directly model the survival times T_{ik} , to objectively compare methods, we use the individual-specific counterfactual survival curve as the basis. That is, the ISTE $\zeta_{a_j, a_{j'}}(\mathbf{x}_{ik})$ will now be defined in a similar way as in equation (3) but using functionals of the counterfactual survival curve – either the survival probability at a fixed point in time or the conditional restricted mean survival time (RMST).⁴¹ We will compare each method's ability to accurately estimate the ISTE $\zeta_{a_j, a_{j'}}(\mathbf{x}_{ik})$ and the average subgroup treatment effect $M(S_{a_j, a_{j'}}^h)$. The performance metrics used to evaluate the methods were the relative bias (or percent bias), root-mean-squared-error (RMSE) and precision in the estimation of heterogeneous effects (PEHE).³ The relative bias evaluates the bias in the estimation of treatment effect on the relative scale with respect to the true treatment effect (which is constant across different methods). The PEHE measures the difference between the true and estimated survival probabilities or RMST across all data points. A smaller value of PEHE indicates a higher estimation accuracy.

For weighting based methods IPW-riCox and DR-riAH, we used Super Learner⁴² to estimate the stabilized inverse probability of treatment weights. Super Learner was implemented using the R package `SuperLearner` and the library argument was set to `SL.library = c("SL.xgboost", "SL.bartMachine", "SL.gbm")`. We used R package `coxme` to implement IPW-riCox and `timereg` to implement DR-riAH. For PEAMM, the `gam` function from R package `mgcv` and two helper functions, (`as_ped` and `add_surv_prob`), from R package `pamtools` were used. For all methods, all confounding variables available to the analyst in their original forms were included in the corresponding models.

4.1.1 Simulation design We simulated datasets with structures similar to the COVID-19 data used in our case study (Section 5). We generated $K = 10$ clusters, each with a sample size of $n_k = 200$. The total sample size is $N = 2000$. We simulated 7 confounding variables for each individual i in cluster k : five continuous variables $X_{ikl} \sim N(0, 1)$, $l \in \{1, \dots, 5\}$; and two categorical variables $X_{ikl} \sim \text{Multinomial}(1, .3, .3, .4)$, $l = 6, 7$. We generated $J = 3$ treatment groups with unequal sample sizes; the ratio of individuals across treatment groups was 5:3:1, which is similar to the ratio of individuals across the three treatment groups in our case study. The treatment assignment mechanism follows a random-intercept multinomial logistic regression model,

$$\begin{aligned} \ln \frac{P(A_{ik} = 1)}{P(A_{ik} = 3)} &= 1.5 + .1X_{ik1} + .1X_{ik2} + .1X_{ik3} + .5X_{ik4} + .4X_{ik5} + .2X_{ik6} + .3X_{ik7} + .4X_{ik2}^2 + .4X_{ik2}^2X_{ik5} + \tau_k \\ \ln \frac{P(A_{ik} = 2)}{P(A_{ik} = 3)} &= .7 + .1X_{ik1} + .3X_{ik2} + .2X_{ik3} + .2X_{ik4} + .1X_{ik5} + .4X_{ik6} + .5X_{ik7} - .3X_{ik2}X_{ik4} + .7X_{ik2}^2X_{ik4} + \tau_k, \end{aligned}$$

where the random intercept $\tau_k \sim N(0, 1^2)$. The parameter setup induces a moderate level of confounding, leading to moderate covariate overlap. The sparsity of overlap can be visualized by the distributions of true generalized propensity scores, shown in Web Figure 1. This moderate covariate overlap mimics the overlap level observed in the COVID-19 dataset (Web Figure xx). Following strategies^{3,43} recommended for assessing the performance of methods in estimating heterogeneous treatment effects, we subclassified the simulated individuals into 40 subgroups based on the distribution of true generalized propensity scores,⁴⁴ and calculated the biases and RMSE for each subgroup across 250 data replications. Note that the generalized propensity scores for each individual sum to one, $P(A_{ik} = 1 | \mathbf{X}_{ik}, \tau_k) + P(A_{ik} = 2 | \mathbf{X}_{ik}, \tau_k) + P(A_{ik} = 3 | \mathbf{X}_{ik}, \tau_k) = 1$. The subclassification is based on intervals of the true generalized propensity scores for treatment 1 and treatment 2, representing a full range of assignment propensity to each treatment group. Subclasses of generalized propensity scores are presented in Web Table 1.

We simulated three sets of true counterfactual survival times from the Weibull survival distribution, which can be parameterised as both the accelerated failure time model and Cox proportional hazards model,¹

$$S_{ik}(t) = \exp \left[- \left\{ \lambda_{a_j} \exp \left(q_{a_j}(\mathbf{X}_{ik}, b_k) \right) t \right\}^\eta \right],$$

where λ_{a_j} is a treatment group specific parameter, η is the shape parameter and $q_{a_j}(\mathbf{X}_{ik}, b_k)$ represents a general functional form of covariates and the random-intercept. Using the inverse transform sampling, we generated counterfactual survival times by

$$T_{ik}(a_j) = \left\{ \frac{-\log U}{\lambda_{a_j} \exp(q_{a_j}(\mathbf{X}_{ik}, b_k))} \right\}^{1/\eta} \quad (7)$$

for $a_j \in \{1, 2, 3\}$, where U is a random variable following the uniform distribution on the interval $[0, 1]$ and $\lambda_{a_j} = \{5000, 800, 1200\}$ for $a_j = 1, 2, 3$. Observed and uncensored survival times are generated as

$$T_{ik} = \sum_{a_j \in \{1, 2, 3\}} T_{ik}(a_j) I(A_{ik} = a_j).$$

We considered three treatment effect heterogeneity settings with an increasing level of complexity:

- (a) $q_1(\mathbf{X}_{ik}, b_k) = .1X_{ik1} + .3X_{ik2} + \sin(\pi X_{ik3}) + .6X_{ik4} + .5X_{ik5} + 1.2X_{ik6} + .4X_{ik7} + .3X_{ik2}^2 + .5X_{ik4}X_{ik5} + b_k - 1$
 $q_2(\mathbf{X}_{ik}, b_k) = .4X_{ik1} + 1.2\sin(\pi X_{ik2}) + .4X_{ik3} + .3X_{ik4} + 1.0X_{ik5} + .8X_{ik6} + .2X_{ik7} + .7X_{ik1}^2 + .4X_{ik1}X_{ik4} + b_k$
 $q_3(\mathbf{X}_{ik}, b_k) = .4X_{ik1} + .9X_{ik2} + .4X_{ik3} + .9X_{ik4} + .4X_{ik5} + .4X_{ik6} + .3X_{ik7} + b_k - 2$
- (b) $q_1(\mathbf{X}_{ik}, b_k) = .1X_{ik1} + .3X_{ik2} + \sin(\pi X_{ik3}) + .6X_{ik4} + .5X_{ik5} + 1.2X_{ik6} + .3X_{ik7} + .3X_{ik2}^2 + .5X_{ik4}X_{ik5} + b_k - 1$
 $q_2(\mathbf{X}_{ik}, b_k) = .4X_{ik1} + 1.2\sin(\pi X_{ik2}) + .4X_{ik3} + .3X_{ik4} + 1.0X_{ik5} + .8X_{ik6} + .1X_{ik7} + .7X_{ik1}^2 + .4X_{ik1}X_{ik4} + b_k$
 $q_3(\mathbf{X}_{ik}, b_k) = .4\sin(\pi X_{ik1}) + .9X_{ik2} + .9X_{ik3} + .4X_{ik4} + .4X_{ik5} + .9X_{ik6} + .3X_{ik7} + .4X_{ik4}^2 - .3X_{ik2}X_{ik3} + b_k - 3$
- (c) $q_1(\mathbf{X}_{ik}, b_k) = .1X_{ik1} + .3X_{ik2} + \sin(\pi X_{ik3}) + .6X_{ik4} + .5X_{ik5} + 1.2X_{ik6} + .3X_{ik2}^2 + .5X_{ik4}X_{ik5} + b_k - 1$
 $q_2(\mathbf{X}_{ik}, b_k) = .4X_{ik1} + 1.2\sin(\pi X_{ik3}) + .4X_{ik4} + .3X_{ik5} + 1.0X_{ik6} + .8X_{ik7} + .7X_{ik1}^2 + .4X_{ik1}X_{ik4} + b_k$
 $q_3(\mathbf{X}_{ik}, b_k) = .4\sin(\pi X_{ik2}) + .9X_{ik3} + .9X_{ik4} + .4X_{ik5} + .4X_{ik6} + .9X_{ik7} + .4X_{ik4}^2 - .3X_{ik2}X_{ik3} + b_k - 3,$

where the random intercept $b_k \sim N(0, 4^2)$. Across all three heterogeneity settings, $X_{ik3}, X_{ik4}, X_{ik5}, X_{ik6}$ were confounders related to both the treatment assignment mechanism and the potential outcome generating process. In scenario (a), nonlinear covariate effects are present in treatment groups 1 and 2. In scenario (b), there are nonlinear covariate effects in all three treatment groups. Scenario (c) is similar to scenario (b) except that a nonoverlapping set of covariates are included in three treatment groups. This additional complexity represents an additional source of treatment effect heterogeneity. The parameter η was set to 2 and $\exp(0.7 + 0.5x_{ik1})$ to respectively induce proportional hazards and nonproportional hazards. We further generate the censoring time C independently from an exponential distribution with the rate parameter chosen to induce a censoring proportion of 50%, which is close to the censoring proportion observed in the COVID-19 data in our case study. The Kaplan-Meier survival curves by treatment group for all three heterogeneity settings under both proportional and nonproportional hazards are presented in Web Figure 2.

4.1.2 Simulation results Table 1 summarizes the overall precision measure PEHE (based on 3-week survival probability) for each of four methods under three heterogeneity settings and both proportional and nonproportional hazards. First, flexible methods riAFT-BART and PEAMM and doubly robust weighting method DR-riAH yielded substantially smaller PEHE than the parametric single robust method IPW-riCox across all simulation scenarios. Second, as the heterogeneity setting became more complex, flexible methods riAFT-BART and PEAMM tended to have better performance evidenced by decreasing mean and variation of the PEHE. All methods show decreasing precision in estimating ISTE, demonstrated by increasing PEHE value, when the proportional hazards assumption fails to hold. This is possibly due to more complex data generating processes, in which the rate parameter η depends on covariate x_{ik1} . The decrease in estimation precision is the smallest for riAFT-BART. Overall, across all scenarios, the proposed method riAFT-BART had the smallest PEHE, or the highest accuracy in estimating the ISTE. Similar observations can be made from the PEHE measures based on 3-week RMST, which are provided in Web Table 2.

Figure 1 displays the relative biases and RMSE results among 40 generalized propensity score subgroups, each averaged across 250 simulation runs. Three pairwise treatment effects were estimated by averaging the ISTE $\hat{\zeta}_{a_j, a_{j'}}(\mathbf{x}_{ik})$ (based on 3-week survival probability) across individuals in each subgroup. Under both settings of proportional hazards and nonproportional hazards, the proposed method riAFT-BART boasts the smallest biases and RMSE across all three treatment effects, particularly for subpopulation near the centroid of the generalized propensity score distribution. In sharp contrast, IPW-riCox, which encodes parametric and linearity assumptions and assumes proportional hazards, yielded the largest biases and RMSE. The increasing complexity level of treatment effect heterogeneity did not impact the performance of more flexible methods PEAMM and riAFT-BART, but induced larger biases and RMSE for parametric methods IPW-riCox and DR-riAH. The violation of the proportional hazards assumption, which introduced an additional data complexity (the rate parameter η depends on the covariate x_{ik1}), had a negligible effect on the performance of riAFT-BART, but all three comparison methods had a deteriorated performance. It is worth noting that all methods produced large biases and RMSE for subpopulation at the tail regions of the generalized propensity score distribution, suggesting that causal inferences drawn about this subpopulation may not be reliable. Results based on 3-week RMST, shown in Web Figure 3, convey the same messages.

4.2 Variable selection

We adopt the simulation settings used in Hu et al.¹² to evaluate the performance of variable selection methods among incomplete, clustered survival data. We used the multivariate amputation approach⁴⁵ to generate missing data scenarios with desired missingness percentages under the missing at random mechanism. The multivariate amputation proceeds through the following three steps: (i) randomly divide the complete data into a certain number of subsets, each allowing the specification of any missing data pattern; (ii) calculate the weighted sum scores for individuals in each subset to amputate the data.

A

Heterogeneity setting (a) (b) (c)

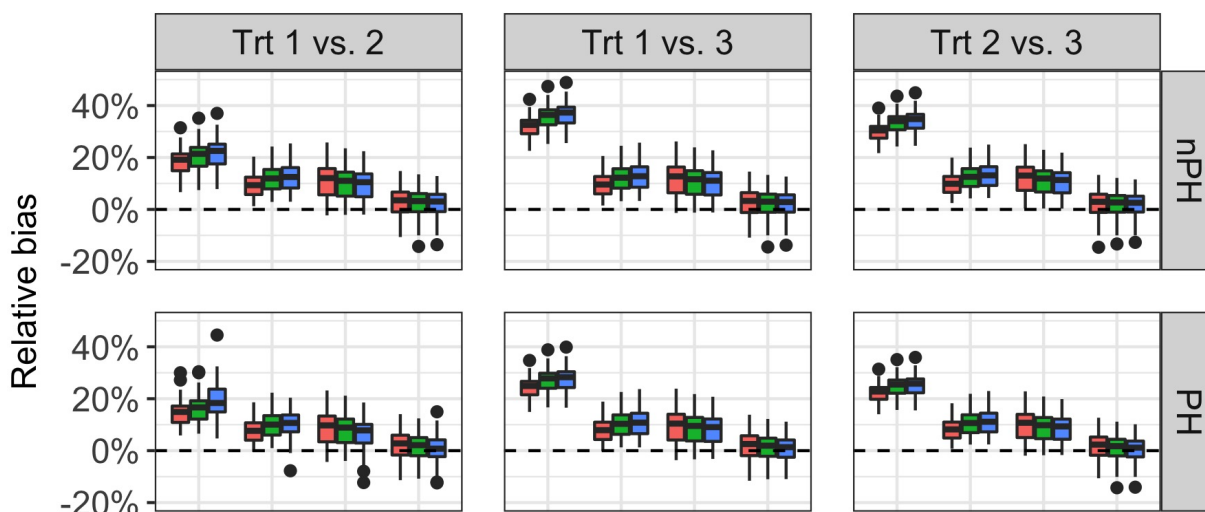
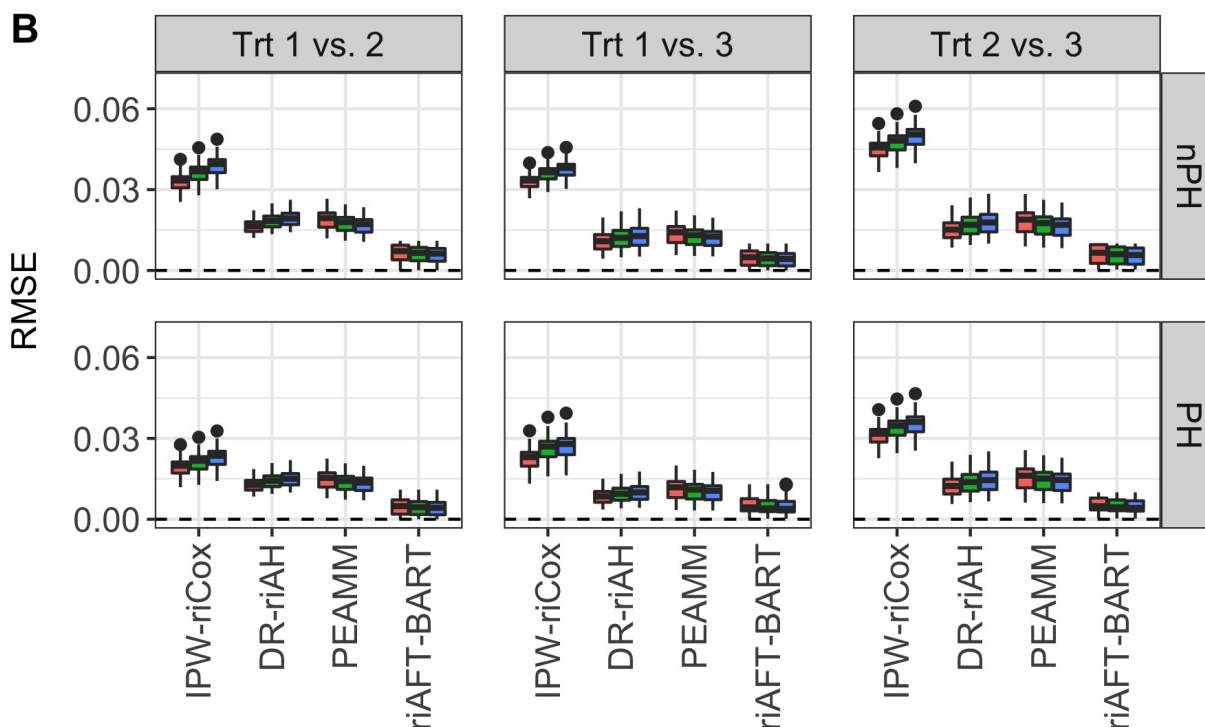
**B**

Figure 1. Relative biases (Panel A) and root-mean-squared-errors (RMSE) (Panel B) among 40 generalized propensity score subgroups under 6 data configurations: (heterogeneity settings a, b, c) \times (proportional hazards (PH) and nonproportional hazards (nPH)) for each of four methods, IPW-riCox, DR-riAH, PEAMM and riAFT-BART. Three pairwise treatment effects were estimated by averaging the individual survival treatment effect (based on 3-week survival probability) across individuals in each subgroup. Each boxplot visualizes the distribution of relative biases or the distribution of RMSE for 40 subgroups, each averaged across 250 simulation runs.

The weighted sum score relates the variable to be amputated to the variables on which the missingness in the amputated variable depends; (iii) apply a logistic distribution function⁴⁶ on the weighted sum scores to compute the missingness probability, which is used to determine whether the data point becomes missing or not. We investigated the practical operating characteristics of our proposed variable selection method using riAFT-BART, and compare it to PEAMM, frailty models with penalized likelihood (FrailtyPenal), frailty models with penalized profile h-likelihood (FrailtyHL) and backward stepwise

Table 1. Mean and (standard deviation) of precision in the estimation of heterogeneity effects (PEHE) across 250 data replications for each of the 4 methods based on 3-week survival probability under six configurations: (proportional hazards [PH] vs. nonproportional hazards [nPH]) \times (heterogeneity setting [HS] (a) vs. (b) vs. (c)).

	Methods	PH			nPH		
		HS(a)	HS(b)	HS(c)	HS(a)	HS(b)	HS(c)
Trt 1 vs. 2	IPW-riCox	.061 (.028)	.067 (.029)	.070 (.030)	.082 (.028)	.089 (.029)	.092 (.030)
	DR-riAH	.018 (.021)	.020 (.022)	.026 (.023)	.028 (.020)	.033 (.021)	.035 (.021)
	PEAMM	.028 (.023)	.024 (.022)	.020 (.021)	.038 (.024)	.034 (.023)	.031 (.023)
	riAFT-BART	.012 (.010)	.009 (.009)	.006 (.009)	.017 (.012)	.014 (.011)	.011 (.011)
Trt 1 vs. 3	IPW-riCox	.065 (.027)	.070 (.028)	.073 (.031)	.083 (.029)	.090 (.030)	.093 (.031)
	DR-riAH	.021 (.018)	.026 (.020)	.029 (.022)	.031 (.019)	.036 (.020)	.039 (.022)
	PEAMM	.035 (.024)	.030 (.023)	.026 (.022)	.049 (.025)	.044 (.024)	.037 (.023)
	riAFT-BART	.016 (.010)	.013 (.009)	.010 (.009)	.022 (.014)	.019 (.013)	.015 (.012)
Trt 2 vs. 3	IPW-riCox	.088 (.030)	.095 (.031)	.098 (.032)	.105 (.031)	.115 (.032)	.118 (.033)
	DR-riAH	.038 (.023)	.043 (.023)	.045 (.024)	.045 (.021)	.050 (.022)	.052 (.022)
	PEAMM	.049 (.023)	.045 (.022)	.041 (.022)	.058 (.024)	.054 (.023)	.049 (.023)
	riAFT-BART	.017 (.012)	.015 (.011)	.013 (.011)	.022 (.015)	.020 (.014)	.018 (.014)

selection with random-intercept Cox regression model (riCox). Four performance metrics were used to evaluate the variable selection results: precision, recall, F_1 and Type I error (Section 3.3).

The multivariate amputation procedure was implemented via the `ampute` function of the R package `mice`.⁴⁵ Imputation was performed using the R package `mice`.⁴⁷ To implement our proposed method using riAFT-BART, we used 4500 posterior draws with the first 1000 discarded as burn-in. The permutation distributions of VIP scores were constructed from 100 riAFT-BART model runs. To implement the variable selection procedure based on PEAMM, we used the helper function (`as.ped`) from R package `pamtools` to reformat the data and used the `gam` function from R package `mgcv` for variable selection. Variable selection by frailty models was implemented using the `frailtyPenal` function of R package `frailtypack` for penalized marginal likelihood; and using the function `frailty.vs` from R package `frailtyHL` for penalized profile h-likelihood. For backward stepwise selection, the random-intercept Cox regression model was fitted using the `coxme` function from R package `coxme`.

4.2.1 Simulation design The simulation scenarios are motivated by the data structures observed in the COVID-19 data set used in our case study. We considered $K = 10$ clusters, each with a sample size of $n_k = 200$. We generated 8 *useful* predictors that are truly related to the survival outcomes, X_{ik1}, \dots, X_{ik8} , and 20 noise predictors, X_{ik9}, \dots, X_{ik28} . We simulated X_{ik1} and X_{ik2} independently from $\text{Bern}(0.5)$, X_{ik3}, X_{ik4} from the standard normal distribution $N(0, 1)$, and $X_{ik5}, X_{ik6}, X_{ik7}, X_{ik8}$ were designed to have missing values under the missing at random mechanism. For a missing at random predictor variable, we specify the true forms in which the predictor depends on the other predictors as the following:

$$\begin{aligned}
 x_{ik5} &| x_{ik2}, x_{ik3} \sim N(0.3x_{ik2} - 0.2x_{ik3}, 1) \\
 x_{ik6} &| x_{ik3}, x_{ik4} \sim N(-0.4x_{ik3} + 0.4x_{ik4} + 0.3x_{ik3}x_{ik4}, 1) \\
 x_{ik7} &| x_{ik4}, x_{ik5}, x_{ik6} \sim N(0.1x_{ik4}(x_{ik5} - 2)^2 - 0.1x_{ik6}^2, 1) \\
 x_{ik8} &| x_{ik5}, x_{ik6}, x_{ik7} \sim N(-0.3x_{ik5}^2 + 0.5x_{ik6} + 0.3x_{ik7} + 0.2x_{ik6}x_{ik7}, 1).
 \end{aligned}$$

Among the 20 noise predictors, 10 were generated as continuous variables $X_{ik9}, \dots, X_{ik18} \stackrel{i.i.d}{\sim} N(0, 1)$, and the other 10 were generated as binary variables $X_{ik19}, \dots, X_{ik28} \stackrel{i.i.d}{\sim} \text{Bern}(0.5)$.

Similar to the outcome generating process described in Section 4.1.1, we generate the observed and uncensored survival times from the Weibull survival distribution,

$$T_{ik} = \left[\frac{-\log U}{\lambda \exp\{q(\mathbf{X}_{ik}, b_k)\}} \right]^{1/\eta}$$

where $\lambda = 3000$, U is a random variable following the uniform distribution on the interval $[0, 1]$, $b_k \sim N(0, 4^2)$, and

$$\begin{aligned}
 q(\mathbf{X}_{ik}, b_k) &= 1.8x_{ik1} + 0.5x_{ik2} + 1.1x_{ik3} - 0.4e^{x_{ik5}} + 0.4(x_{ik6} - 1.5)^2 + 0.1(x_{ik7} - 0.1)^3 \\
 &\quad - 5 \sin(0.1\pi x_{ik4}x_{ik8}) - 0.4x_{ik5}x_{ik7} + b_k
 \end{aligned} \tag{8}$$

We further generated the censoring time C independently from an exponential distribution with the rate parameter selected to induce the censoring proportion of 50%. The parameter η was set to 2 and $\exp(0.7 + 0.5x_{ik1})$ to respectively produce proportional hazards and nonproportional hazards. This data generating process was designed to make it difficult for any method to accurately model the survival outcome. We considered the outcome model with arbitrary data complexity that

reflects common situations in health datasets: (i) discrete predictors with strong (X_{ik1}) and moderate (X_{ik2}) associations; (ii) both linear and nonlinear forms of continuous predictors (X_{ik6} and X_{ik7}); (iii) nonadditive effects ($X_{ik4}X_{ik8}$).

After generating the fully observed data, we amputated the four predictors designed to have missing values X_{ik5} , X_{ik6} , X_{ik7} , X_{ik8} under the missing at random mechanism using the multivariate amputation approach. Additional technical details for the amputation procedure are available in Schouten et al.;⁴⁵ and additional amputation details for the simulation appear in Web Section 2. The resultant simulation data have an overall missingness proportion of 40%.

4.2.2 Simulation results Table 2 summarizes variable selection results by each method. The optimal performance among incomplete data is shown for the best selection threshold value of π – chosen on the basis of the F_1 score (see Web Figures 4-5); and is compared against the performance on fully observed data (before amputation) and among complete cases only. The proposed method riAFT-BART has the best performance across all three data panels (fully observed, with missing data, complete cases), evidenced by the highest precision, recall and F_1 score, and the lowest type I error. The second best performing method is PEAMM, for its modeling flexibility over parametric methods. In the presence of missing covariate data, all methods had a slightly deteriorated performance when performing variable selection in combination with bootstrap imputation, but the performance of variable selection among only complete cases was considerably lower.

Table 2. Simulation results for each variable selection approach performed on the fully observed data, and among incomplete data with 40% overall missingness in covariates under proportional hazards and non-proportional hazards. Imputation was conducted via *mice*. For each of five methods, we show results corresponding to the best threshold values of π (based on F_1).

	Proportional hazards					Non-proportional hazards			
	Precision	Recall	F_1	Type I error		Precision	Recall	F_1	Type I error
Fully observed data									
riAFT-BART	0.95	0.88	0.91	0.01	riAFT-BART	0.93	0.87	0.89	0.02
PEAMM	0.83	0.82	0.82	0.02	PEAMM	0.81	0.80	0.80	0.03
FrailtyHL	0.81	0.78	0.79	0.03	FrailtyHL	0.78	0.71	0.74	0.04
FrailtyPenal	0.79	0.76	0.77	0.04	FrailtyPenal	0.75	0.69	0.72	0.05
riCox	0.78	0.72	0.75	0.05	riCox	0.72	0.67	0.69	0.05
40% overall missing									
riAFT-BART $\pi = 0.1$	0.93	0.85	0.89	0.02	riAFT-BART $\pi = 0.1$	0.89	0.84	0.86	0.03
PEAMM $\pi = 0.7$	0.88	0.74	0.80	0.03	PEAMM $\pi = 0.6$	0.84	0.72	0.78	0.04
FrailtyHL $\pi = 0.6$	0.79	0.73	0.76	0.05	FrailtyHL $\pi = 0.7$	0.75	0.70	0.71	0.04
FrailtyPenal $\pi = 0.6$	0.76	0.71	0.74	0.04	FrailtyPenal $\pi = 0.7$	0.72	0.67	0.69	0.05
riCox $\pi = 0.8$	0.85	0.67	0.73	0.04	riCox $\pi = 0.7$	0.71	0.63	0.68	0.07
Complete cases									
riAFT-BART	0.85	0.81	0.83	0.03	riAFT-BART	0.83	0.79	0.81	0.04
PEAMM	0.77	0.73	0.75	0.02	PEAMM	0.73	0.71	0.72	0.03
FrailtyHL	0.73	0.68	0.71	0.04	FrailtyHL	0.70	0.65	0.67	0.05
FrailtyPenal	0.71	0.65	0.69	0.05	FrailtyPenal	0.69	0.62	0.65	0.04
riCox	0.71	0.66	0.68	0.04	riCox	0.66	0.62	0.64	0.03

Demonstrated by Figure 2, the proposed method riAFT-BART tended to select the most useful predictors and the least noise predictors, followed by another flexible method PEAMM, under both proportional hazards and non-proportional hazards. Among parametric methods, penalized likelihood methods for frailty models had slightly better performance than riCox. All methods tended to select more noise predictors and less useful predictors under non-proportional hazards; the decrease in the performance due to elevated data complexity associated with nonproportional hazards, was only marginal for riAFT-BART but considerable for less flexible methods, particularly FrailtyHL and riCox.

A perusal of each method's ability to select each of useful predictors is visualized in Figure 3. All methods had a good power (> 0.8) for selecting a strong discrete predictor (X_{ik1}), but unsatisfactory power (< 0.5) for detecting a discrete predictor (X_{ik2}) that only has a moderate relationship with the outcome. For continuous variables, all methods performed well in selecting X_{ik3} , which has only a linear relationship with the log survival time, but riAFT-BART produced a significantly higher power for selecting the predictor X_{ik4} , which has a complex nonadditive form in model (8). Among the four predictors with missing data X_{ik4}, \dots, X_{ik8} , the advantage of riAFT-BART is demonstrated by the higher power of selecting predictors that have more complex functional forms that are difficult to be captured by other methods considered. A direct comparison of the proportional hazards setting with nonproportional hazards shows that all methods performed better under proportional hazards, but the impact of the violation of proportional hazards is the smallest for riAFT-BART.

As our proposed method riAFT-BART pivots on the predictor's VIP, we examined the convergence of the Markov chain by plotting 4500 posterior draws, with the first 1000 discarded as burn-in, of the VIP for four useful predictors and four noise predictors in Web Figure 6. The method converged well.

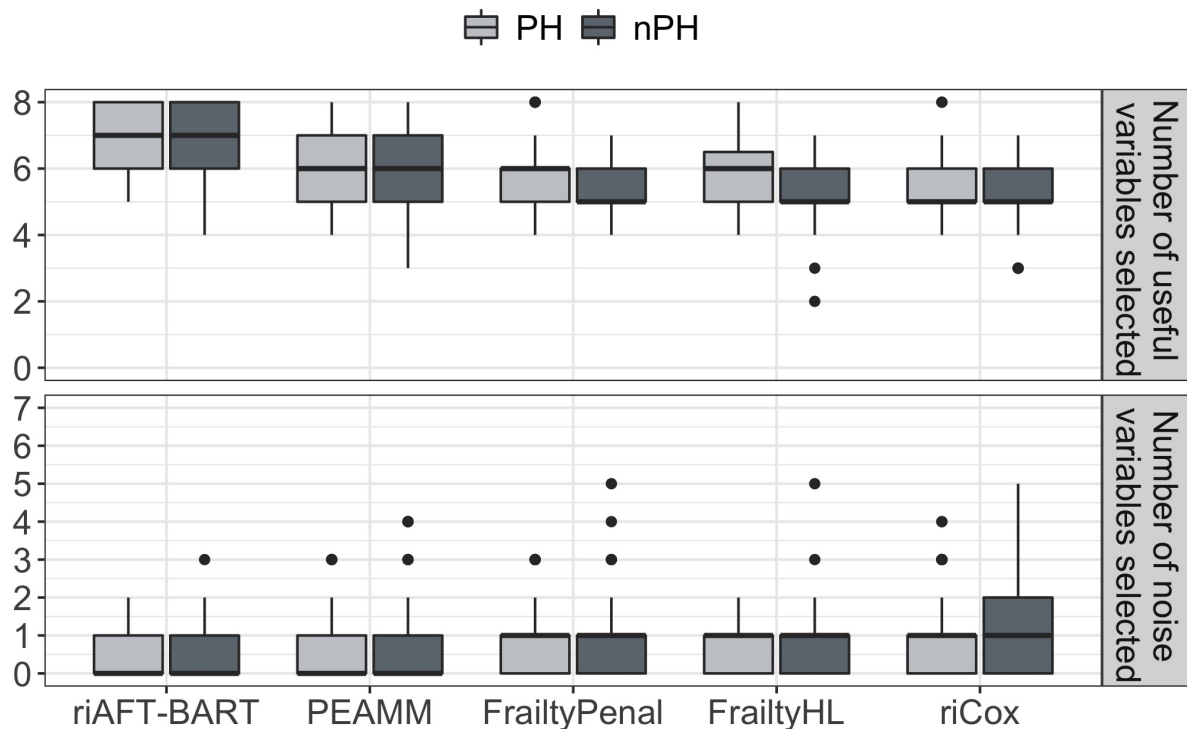


Figure 2. The distribution, across 250 data replications, of the numbers of selected noise predictors and useful predictors for each of five methods: riAFT-BART, PEAMM, FrailtyHL, FrailtyPenal and riCox, with clustered survival data generated under both proportional hazards (PH) and non-proportional hazards (nPH). The total number of useful predictors is 8 and the total number of noise predictors is 20. There are $K = 10$ clusters, each with a size of 200; the total sample size is 2000. The overall proportion of missingness is 40%.

5 Case study: Predictors for in-hospital mortality and heterogeneous survival treatment effects among post-ICU COVID patients

In this case study, we first applied the proposed variable selection methods to select important predictors for in-hospital mortality using a comprehensive COVID-19 dataset, and then evaluated the treatment effect heterogeneity on patient survival using the selected predictors by implementing our proposed method riAFT-BART. The COVID-19 dataset was drawn from six hospitals (clusters) of the Epic electronic medical records system at the Mount Sinai Medical Center. Included in this dataset were 1955 patients who were diagnosed with COVID-19 between March 10, 2020 to February 26, 2021 and were in intensive care (ICU) due to COVID-19 during their hospital stay.⁴⁸ Post ICU admission, each patient received COVID-specific medications: either dexamethasone, or remdesivir, or the combination of dexamethasone and remdesivir (dexamethasone+remdesivir). The cluster sizes and number of patients in each treatment group are provided in Web Table 4.

We used the following 28 baseline (time of ICU admission) variables: age, sex, self-reported race and ethnicity, smoking status, binary comorbidities including hypertension, coronary artery disease, cancer, diabetes, asthma, and chronic obstructive pulmonary disease, vital signs (measured within 24 hours of ICU admission) including temperature, systolic blood pressure, diastolic blood pressure, patient oxygen level (see Web Table 3 for definition), heart rate, the fraction of inspired oxygen, body mass index, oxygen saturation, risk score (sequential organ failure assessment score and glasgow coma scale), laboratory test results including partial pressure of oxygen, D dimer value and inflammatory markers such as lactate dehydrogenase, ferritin, c-reactive protein, creatinine and white blood cell count. In cases where multiple vital signs/risk score/lab results were recorded during the first 24 hours of ICU admission, we used the mean value of the multiple measurements. Among the 28 candidate predictor variables, 17 variables have missing data and the missingness proportion ranges from 1.4% to 28.6%. Only 1187 (60.7%) patients have fully observed data for all covariates, which motivated the overall missingness proportion of 40% used in our simulation study (Section 4.2). Detailed summary statistics for baseline variables appear in Web Table 4.

The Kaplan-Meier survival curves by treatment group are displayed in Web Figure 7, with crossovers suggesting nonproportional hazards. Assessed by the distribution of the generalized propensity scores shown in Web Figure 8, there is moderate covariate overlap across three treatment groups in the COVID-19 data.

We first implemented all five variable selection methods. All 28 candidate predictors were included in the imputation models, and the optimal threshold value of π for each method, which produced the best F_1 score in the simulation study, was

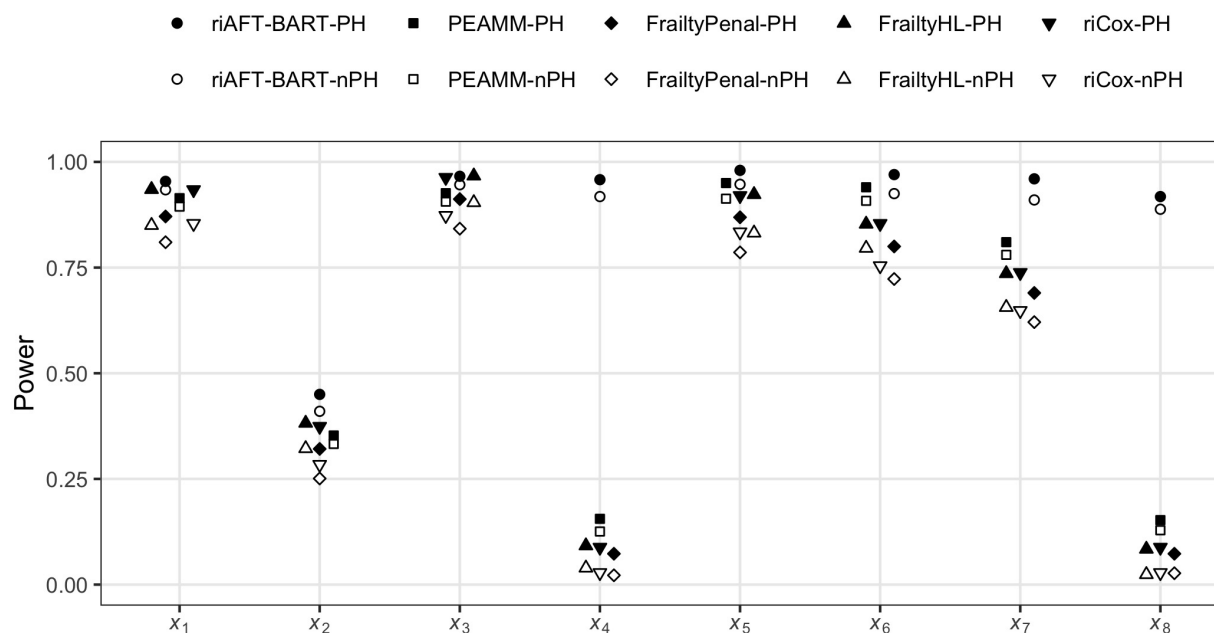


Figure 3. Power of each of five methods: riAFT-BART, PEAMM, FrailtyHL, FrailtyPenal and riCox, for selecting each of 8 useful predictors with clustered survival data generated under proportional hazards (PH) and non-proportional hazards (nPH), based on 250 data replications. There are $K = 10$ clusters, each with a size of 200; the total sample size is 2000. The overall proportion of missingness is 40%. Filled symbols represent the PH setting, and open symbols correspond to the nPH setting.

Table 3. Variable selection results by each of 5 methods, with the best selection threshold value of π suggested in simulations under non-proportional hazards. riAFT-BART and riCox both selected 8 variables, PEAMM selected 7 variables, FrailtyPenal selected 6 variables and FrailtyHL selected 9 variables.

Variables	riAFT-BART	PEAMM	FrailtyPenal	FrailtyHL	riCox
Oxygen level	Yes	Yes	No	Yes	Yes
Age	Yes	Yes	Yes	Yes	No
Creatinine	Yes	Yes	No	Yes	Yes
White blood cell	Yes	Yes	No	No	Yes
SOFA score	Yes	Yes	Yes	Yes	No
Race	Yes	No	Yes	Yes	Yes
D dimer	Yes	No	No	Yes	No
LDH	Yes	Yes	Yes	Yes	Yes
C-reactive protein	No	Yes	No	Yes	Yes
Ferritin	No	No	No	Yes	Yes
Oxygen saturation	No	No	Yes	No	No
Glasgow coma scale	No	No	Yes	No	Yes

Abbreviations: LDH = Lactate dehydrogenase; SOFA = Sequential organ failure assessment

used to select the final set of predictors. As summarized in Table 3, FrailtyHL selected the most (9) predictors, riAFT-BART and riCox both selected 8 predictors, PEAMM selected 7 predictors and FrailtyPenal selected the least (6) predictors. Age and lactate dehydrogenase were the only two predictors selected by all five methods. Variables selected by the two flexible methods riAFT-BART and PEAMM were largely in agreement with each other, with the exception that riAFT-BART but not PEAMM selected Race and D dimer, and PEAMM but not riAFT-BART selected C-reactive protein.

To further distinguish between methods based on their ability to select the most relevant predictors, we computed the predictive performance of the five methods that modeled the outcome variable on their respectively selected predictor variables. For survival outcomes, we used the concordance statistic as a metric to assess the predictive performance.⁴⁹ The concordance statistic is the fraction of concordant pairs among all pairs of individuals. A pair of patients is called concordant if the patient with lower (higher) predicted survival probability at a given time point had a longer (shorter) time to death. In this case study, we chose 21 days post ICU admission as the target time point, because it is a sufficiently long time to evaluate the effects of COVID-19 treatments on in-hospital mortality for severe patients. As the COVID-19 dataset is subject to missing covariate data, to calculate the cross validated concordance statistic, we follow the strategy described in Lin et al.²⁹

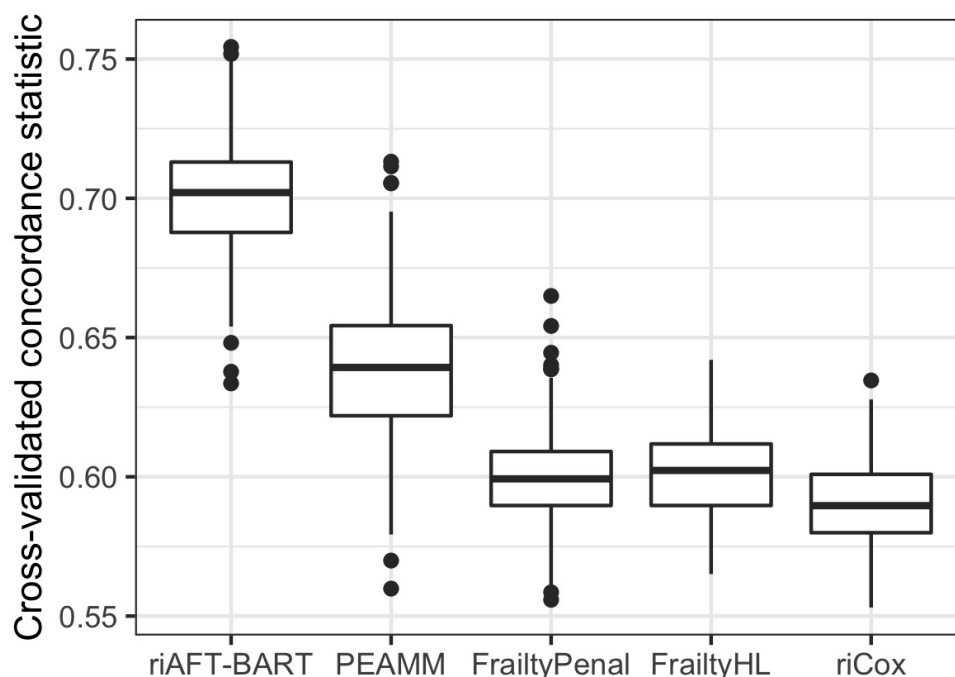


Figure 4. The distribution of cross-validated concordance statistics across 250 data replications for each of five methods using the COVID-19 dataset.

We first split the data into two halves and implemented each of the five variable selection methods on half of the data. Then we imputed the other half of the data with a single imputation and recorded the concordance statistic. Finally we repeated the previous two steps 250 times to get the distribution of the cross-validated concordance statistics. Figure 4 shows that the proposed method riAFT-BART yielded the highest predictive performance with a median concordance statistic > 0.7 .

Supported by both the simulation study and case study, riAFT-BART provided the best variable selection results. Thus we used the 8 predictors selected by riAFT-BART as confounding variables, and estimated the heterogeneous treatment effects on patient survival using methodology described in Section 2. To address the missing data issue when drawing causal inferences about treatment effects, we fitted an riAFT-BART model (1) on each of the 100 bootstrap and imputed datasets (previously conducted for variable selection), and drew statistical inferences about the ISTE $\zeta_{a_j, a_{j'}}(\mathbf{x}_{ik})$, defined in equation (3), by pooling posterior samples of the ISTE, $\tilde{f}^d(a_j, \mathbf{x}_{ik}) - \tilde{f}^d(a_{j'}, \mathbf{x}_{ik})$ as in equation (2), across model fits arising from the multiple datasets.^{50,51} Inferences about the population average treatment effects $\theta_{a_j, a_{j'}}$ can be obtained from the posterior samples of $\tilde{f}^d(a_j, \mathbf{x}_{ik}) - \tilde{f}^d(a_{j'}, \mathbf{x}_{ik})$ across the sample population.¹ The population average treatment effects, summarized in Web Table 5, suggest that there was no statistically significant difference in treatment effect when comparing dexamethasone with remdesivir or with a combined use of dexamethasone and remdesivir. However, there was a statistically significant treatment benefit associated with dexamethasone+remdesivir compared to using remdesivir alone. Web Figure 9 demonstrates that substantial variability in the institutional effect was captured by the riAFT-BART model: the Mount Sinai main hospital had considerably better outcomes than the Mount Sinai Queens hospital.

Turning to the treatment effect heterogeneity. Figure 5 summarizes the combination rules of covariates $\mathcal{S}_{a_j, a_{j'}}$ that have differential subgroup treatment effect $\mathcal{M}(\mathcal{S}_{a_j, a_{j'}})$, defined in equation (4), than the sample population treatment effect. When comparing remdesivir and dexamethasone + remdesivir across the sample population, there was significant treatment benefit, suggested by a longer expected survival time, for the combined use of dexamethasone and remdesivir. Our analysis suggests that combining dexamethasone and remdesivir offered enhanced treatment benefit for relatively healthier COVID-19 patients with lower oxygen saturation ($< 95.5\%$) and a normal white blood cell count ($< 11.4K/\mu L$), demonstrated by the leftmost branch of the tree diagram in Figure 5. By contrast, the rightmost branch suggests that there was no statistically significant treatment benefit associated with either treatment choice for comparatively unhealthier patients with a higher level of oxygen saturation ($> 95.5\%$).

6 Discussion

We describe two important and practical utilities of a new Bayesian machine learning tool riAFT-BART for analyzing clustered and censored survival data. To address the implications of complex data structures of large-scale clinical datasets generated from multiple institutions for causal inferences about population treatment effect, riAFT-BART was developed

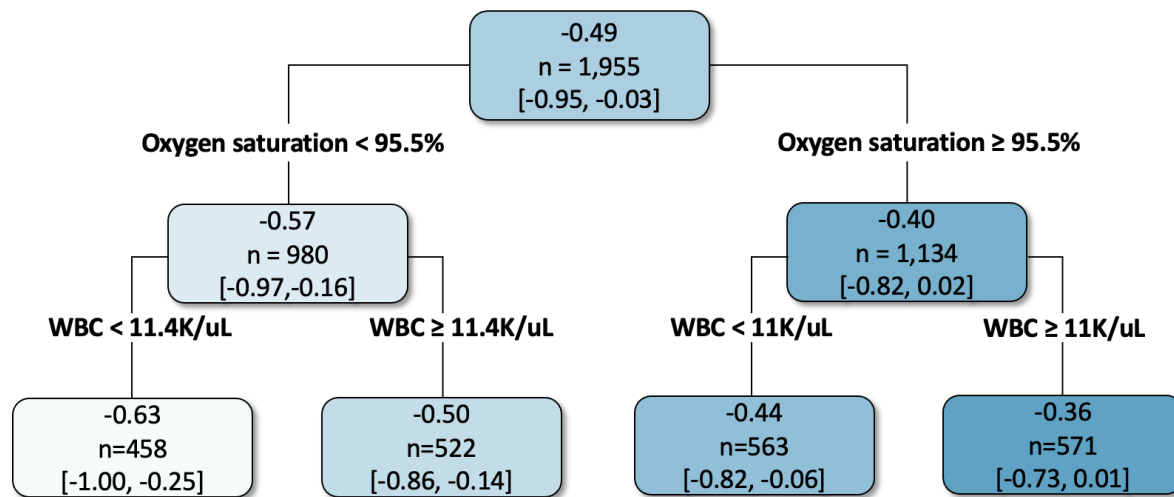


Figure 5. Final Random Forests model fit to the posterior mean of the individual survival treatment effect comparing remdesivir and dexamethasone + remdesivir. Values in each node correspond to the posterior mean, in terms of difference in log survival days, for the subgroup of individuals represented in that node. Uncertainty intervals were obtained by pooling the posterior samples arising from the multiple imputed data sets. WBC: White blood cell.

to accurately estimate the population average treatment effect on patient survival while accounting for the variation in institutional effects.¹ Moving from broad applicability of a population study to personalized medicine requires the understanding of treatment effect heterogeneity. The treatment effect heterogeneity was traditionally identified by first enumerating potential effect modifiers with subject-matter experts and then estimating the average treatment effect within each subgroup.⁵² This approach is particularly suitable to confirmatory treatment effect heterogeneity analysis in randomized clinical trials. In observational data with a large number of pre-treatment covariates, such *a priori* specification that separates the issues of confounding and treatment effect heterogeneity is often practically infeasible. We described a way in which the new tool riAFT-BART can be used to perform an exploratory treatment effect heterogeneity analysis to generate scientifically meaningful hypotheses and treatment effect discovery. Through a comprehensive simulation representative of complex confounding and heterogeneity settings with right-censored survival data, we provided new empirical evidence for the better performance of our proposed method in comparison with three existing methods. In the application to a large COVID-19 dataset, we found that oxygen saturation and white blood cell count were two key patient factors that modulated the comparative treatment effect between remdesivir and dexamethasone + remdesivir. We further exploited the posterior samples of the ISTE from riAFT-BART and the random forests model to explore clinically meaningful relationships between COVID-19 medications, patient profile and expected survival time. The results could facilitate treatment effect discovery in subpopulations and may inform personalized treatment strategy and the planning of future confirmatory randomized trials.

Drawing on prior work¹² that combines bootstrap imputation and BART for variable selection among incomplete data, we develop a way in which riAFT-BART can be used to select important predictors among incomplete, clustered and censored survival observations. This strategy is general enough to accommodate any missing data pattern and is highly flexible as it leverages BART to model the relationship between survival times and covariates. As demonstrated by both simulations and the case study, this elevated modeling flexibility gave rise to substantially better variable selection results, particularly in terms of identifying predictors of complex functional forms, compared to existing variable selection methods suitable for clustered survival data.

There are several important avenues for further research. First, the riAFT-BART model could be extended to include the random slopes and accommodate the cluster-level covariates. Correspondingly, a variable selection method can be developed to identify important predictors at both the individual level and the cluster level. Second, using flexible modeling techniques alone will not address violations of the no unmeasured confounding assumption required for causal inference. Developing a formal sensitivity analysis approach⁵¹ for unmeasured confounding would be a worthwhile and important contribution. Finally, our bootstrap imputation-based variable selection procedure is computationally demanding on a large dataset. Although the bootstrap resampling can be computed in parallel on multiple cores when such resources are available, it would be worthwhile to develop strategies that could offer substantial computational savings.

Data Availability Statement

R codes to implement our proposed methods and the comparison methods, and to replicate our simulation studies are provided in the GitHub page of the author <https://github.com/liangyuanhu/TEH-VS-riAFTBART>, and are also available in the R package riAFTBART. Access to the COVID-19 data used in the case study needs to be requested and approved by the Icahn School of Medicine at Mount Sinai.

Declaration of conflicting interests

The authors declare that they have no conflict of interest.

Funding

This work was supported in part by award ME.2017C3.9041 from the Patient-Centered Outcomes Research Institute, and by grants R21CA245855 and 1R01HL159077-01A1 from the National Institute of Health.

References

1. Hu L, Ji J, Ennis RD et al. A flexible approach for causal inference with multiple treatments and clustered survival outcomes. *arXiv preprint* 2022; ArXiv:2202.08318.
2. Chipman HA, George EI and McCulloch RE. BART: Bayesian additive regression trees. *The Annals of Applied Statistics* 2010; 4(1): 266–298.
3. Hu L, Ji J and Li F. Estimating heterogeneous survival treatment effect in observational data using machine learning. *Statistics in Medicine* 2021; 40(21): 4691–4713.
4. Fan J and Li R. Variable selection for Cox’s proportional hazards model and frailty model. *The Annals of Statistics* 2002; 30(1): 74–99.
5. Androulakis E, Koukouvinos C and Vonta F. Estimation and variable selection via frailty models with penalized likelihood. *Statistics in Medicine* 2012; 31(20): 2223–2239.
6. Utazirubanda JC, M León T and Ngom P. Variable selection with Group LASSO approach: Application to Cox regression with frailty model. *Communications in Statistics-Simulation and Computation* 2021; 50(3): 881–901.
7. Bender A, Groll A and Scheipl F. A generalized additive model approach to time-to-event analysis. *Statistical Modelling* 2018; 18(3-4): 299–321.
8. Marra G and Wood SN. Practical variable selection for generalized additive models. *Computational Statistics & Data Analysis* 2011; 55(7): 2372–2387.
9. Rondeau V, Commenges D and Joly P. Maximum penalized likelihood estimation in a gamma-frailty model. *Lifetime Data Analysis* 2003; 9(2): 139–153.
10. Marquardt DW. An algorithm for least-squares estimation of nonlinear parameters. *Journal of the Society for Industrial and Applied Mathematics* 1963; 11(2): 431–441.
11. Ha ID, Pan J, Oh S et al. Variable selection in general frailty models using penalized h-likelihood. *Journal of Computational and Graphical Statistics* 2014; 23(4): 1044–1060.
12. Hu L, Joyce Lin JY and Ji J. Variable selection with missing data in both covariates and outcomes: Imputation and machine learning. *Statistical Methods in Medical Research* 2021; 30(12): 2651–2671.
13. Bleich J, Kapelner A, George EI et al. Variable selection for BART: an application to gene regulation. *The Annals of Applied Statistics* 2014; 8(3): 1750–1781.
14. Ishwaran H, Kogalur UB, Gorodeski EZ et al. High-dimensional variable selection for survival data. *Journal of the American Statistical Association* 2010; 105(489): 205–217.
15. Lagani V and Tsamardinos I. Structure-based variable selection for survival data. *Bioinformatics* 2010; 26(15): 1887–1894.
16. Hu L and Hogan JW. Causal comparative effectiveness analysis of dynamic continuous-time treatment initiation rules with sparsely measured outcomes and death. *Biometrics* 2019; 75(2): 695–707.
17. Chen PY and Tsiatis AA. Causal inference on the difference of the restricted mean lifetime between two groups. *Biometrics* 2001; 57(4): 1030–1038.
18. Arpino B and Cannas M. Propensity score matching with clustered data. an application to the estimation of the impact of caesarean section on the apgar score. *Statistics in Medicine* 2016; 35(12): 2074–2091.
19. Hu L, Gu C, Lopez M et al. Estimation of causal effects of multiple treatments in observational studies with a binary outcome. *Statistical Methods in Medical Research* 2020; 29: 3218–3214.
20. Hu L and Gu C. Estimation of causal effects of multiple treatments in healthcare database studies with rare outcomes. *Health Services and Outcomes Research Methodology* 2021; 21(3): 287–308.
21. Gelman A, Van Dyk DA, Huang Z et al. Using redundant parameterizations to fit hierarchical models. *Journal of Computational and Graphical Statistics* 2008; 17(1): 95–122.
22. Henderson NC, Louis TA, Rosner GL et al. Individualized treatment effects with censored data via fully nonparametric bayesian accelerated failure time models. *Biostatistics* 2020; 21(1): 50–68.
23. Foster JC, Taylor JM and Ruberg SJ. Subgroup identification from randomized clinical trial data. *Statistics in Medicine* 2011; 30(24): 2867–2880.
24. Logan BR, Sparapani R, McCulloch RE et al. Decision making and uncertainty quantification for individualized treatments using Bayesian Additive Regression Trees. *Statistical Methods in Medical Research* 2019; 28(4): 1079–1093.
25. Hu L, Lin JYJ, Sigel K et al. Estimating heterogeneous survival treatment effects of lung cancer screening approaches: A causal machine learning analysis. *Annals of Epidemiology* 2021; 62: 36–42.
26. Breiman L. Random forests. *Machine Learning* 2001; 45(1): 5–32.
27. Deng H. Interpreting tree ensembles with intrees. *International Journal of Data Science and Analytics* 2019; 7(4): 277–287.
28. VanderWeele TJ. Principles of confounder selection. *European Journal of Epidemiology* 2019; 34(3): 211–219.
29. Lin JYJ, Hu L, Huang C et al. A flexible approach for variable selection in large-scale healthcare database studies with missing covariate and outcome data. *BMC Medical Research Methodology* 2022; 22: 132.
30. Hu L, Liu B and Li Y. Ranking sociodemographic, health behavior, prevention, and environmental factors in predicting neighborhood cardiovascular health: a Bayesian machine learning approach. *Preventive Medicine* 2020; 141: 106240.
31. Huang J and Ma S. Variable selection in the accelerated failure time model via the bridge method. *Lifetime Data Analysis* 2010; 16(2): 176–195.

32. Hu L, Li L and Ji J. Machine learning to identify and understand key factors for provider-patient discussions about smoking. *Preventive Medicine Reports* 2020; 20: 101238.
33. Hu L, Liu B, Ji J et al. Tree-based machine learning to identify and understand major determinants for stroke at the neighborhood level. *Journal of the American Heart Association* 2020; 9(22): e016745.
34. Tibshirani R. Regression shrinkage and selection via the Lasso. *Journal of the Royal Statistical Society: Series B (Methodological)* 1996; 58(1): 267–288.
35. Fan J and Li R. Variable selection via nonconcave penalized likelihood and its oracle properties. *Journal of the American Statistical Association* 2001; 96(456): 1348–1360.
36. Lee Y and Oh HS. A new sparse variable selection via random-effect model. *Journal of Multivariate Analysis* 2014; 125: 89–99.
37. Wood AM, White IR and Royston P. How should variable selection be performed with multiply imputed data? *Statistics in Medicine* 2008; 27(17): 3227–3246.
38. Cortinas Abrahantes J and Burzykowski T. A version of the EM algorithm for proportional hazard model with random effects. *Biometrical Journal* 2005; 47(6): 847–862.
39. Long Q and Johnson BA. Variable selection in the presence of missing data: resampling and imputation. *Biostatistics* 2015; 16(3): 596–610.
40. Cai J and Zeng D. Additive mixed effect model for clustered failure time data. *Biometrics* 2011; 67(4): 1340–1351.
41. Royston P and Parmar MK. Restricted mean survival time: an alternative to the hazard ratio for the design and analysis of randomized trials with a time-to-event outcome. *BMC Medical Research Methodology* 2013; 13(1): 1–15.
42. Van der Laan MJ, Polley EC and Hubbard AE. Super learner. *Statistical Applications in Genetics and Molecular Biology* 2007; 6(1).
43. Lu M, Sadiq S, Feaster DJ et al. Estimating individual treatment effect in observational data using random forest methods. *Journal of Computational and Graphical Statistics* 2018; 27(1): 209–219.
44. Feng P, Zhou XH, Zou QM et al. Generalized propensity score for estimating the average treatment effect of multiple treatments. *Statistics in Medicine* 2012; 31(7): 681–697.
45. Schouten RM, Lugtig P and Vink G. Generating missing values for simulation purposes: a multivariate amputation procedure. *Journal of Statistical Computation and Simulation* 2018; 88(15): 2909–2930.
46. Van Buuren S. *Flexible imputation of missing data*. 2nd ed. Boca Raton, FL: Chapman & Hall, 2018.
47. Van Buuren, Stef and Groothuis-Oudshoorn, Karin. mice: Multivariate imputation by chained equations in R. *Journal of Statistical Software* 2010; 45(3): 1–67.
48. Hu L, Li F, Ji J et al. Estimating the causal effects of multiple intermittent treatments with application to COVID-19. *arXiv preprint* 2021; ArXiv:2109.13368.
49. Harrell Jr FE, Lee KL and Mark DB. Multivariable prognostic models: Issues in developing models, evaluating assumptions and adequacy, and measuring and reducing errors. *Statistics in Medicine* 1996; 15(4): 361–387.
50. Zhou X and Reiter JP. A note on Bayesian inference after multiple imputation. *The American Statistician* 2010; 64(2): 159–163.
51. Hu L, Zou J, Gu C et al. A flexible sensitivity analysis approach for unmeasured confounding with multiple treatments and a binary outcome with application to SEER-Medicare lung cancer data. *Annals of Applied Statistics* 2022; 16(2): 1014–1037.
52. Kent DM, Paulus JK, Van Klaveren D et al. The predictive approaches to treatment effect heterogeneity (path) statement. *Annals of Internal Medicine* 2020; 172(1): 35–45.

Web-based Supplementary Materials for “A new tool for clustered survival data:
Estimation of treatment effect heterogeneity and variable selection”

Liangyuan Hu

Department of Biostatistics and Epidemiology, Rutgers University School of Public Health, USA

S1 Sampling algorithm of riAFT-BART

With riAFT-BART, a Metropolis within Gibbs procedure was employed for posterior inferences about treatment effects on patient survival. The observed responses y_{ik} were first centered via the following two steps: (i) fit a parametric intercept-only accelerated failure time model assuming log-normal residuals, and estimate the intercept $\hat{\mu}_{AFT}$ and the residual scale $\hat{\sigma}_{AFT}$; (ii) transform the responses as $y_{ik}^{cent} = y_{ik} \exp(-\hat{\mu}_{AFT})$. Using the centered complete-data survival times $y_{ik}^{cent,c}$, the joint posterior is

$$P\left(b_k, \tau^2, \alpha_k, \mu_{lh}, \sigma^2 \mid y_{ik}^{cent,c}, \mathbf{X}_{ik}, A_{ik}, V_k, \{\mathcal{W}_h, \mathcal{M}_h\}\right) \\ \propto P\left(y_{ik}^{cent,c} \mid \mathbf{X}_{ik}, A_{ik}, V_k, b_k, \tau^2, \alpha_k, \sigma^2, \{\mathcal{W}_h, \mathcal{M}_h\}\right) P(b_k \mid \tau^2, \alpha_k) P(\tau^2) P(\alpha_k) P(\mu_{lh}) P(\sigma^2),$$

where \mathcal{W}_h is the h th binary tree structure, $\mathcal{M}_h = (\mu_{1h}, \dots, \mu_{c_h h})^T$ is the set of c_h terminal node parameters associated with tree structure \mathcal{W}_h . For a given value A_{ik} and \mathbf{X}_{ik} in the predictor space, the binary tree function returns the parameter μ_{lh} , $l \in \{1, \dots, c_h\}$ associated with the terminal node of the predictor subspace in which $\{A_{ik}, \mathbf{X}_{ik}\}$ falls.

We can draw the values of BART sum-of-trees model parameters, μ_{lh} and σ^2 , directly from the fitted BART model. Their posterior distributions $P\left(\mu_{lh} \mid y_{ik}^{cent,c}, \mathbf{X}_{ik}, A_{ik}, V_k, b_k, \tau^2, \alpha_k, \sigma^2, \{\mathcal{W}_h\}\right)$ and $P\left(\sigma^2 \mid y_{ik}^{cent,c}, \mathbf{X}_{ik}, A_{ik}, V_k, b_k, \tau^2, \alpha_k, \{\mathcal{W}_h, \mathcal{M}_h\}\right)$ are presented in Web Section S1 of Hu et al. (2022). The posterior distribution of the random intercept b_k is

$$\left[b_k \mid y_{ik}^{cent,c}, \mathbf{X}_{ik}, A_{ik}, V_k, \tau^2, \alpha_k, \sigma^2, \{\mathcal{W}_h, \mathcal{M}_h\}\right] \sim N\left(\frac{\tau^2 \alpha_k \sum_{i=1}^{n_k} (y_{ik}^{cent,c} - \hat{f}(\mathbf{X}_{ik}, A_{ik}))}{n_k \tau^2 \alpha_k + \sigma^2}, \frac{\sigma^2 \tau^2 \alpha_k}{n_k \tau^2 \alpha_k + \sigma^2}\right).$$

The posterior of α_k , used for parameter expansion, is

$$\left[\alpha_k \mid y_{ik}^{cent,c}, \mathbf{X}_{ik}, A_{ik}, V_k, \tau^2, b_k, \sigma^2, \{\mathcal{W}_h, \mathcal{M}_h\}\right] \sim IG\left(1, 1 + \frac{\sum_{k=1}^K b_k^2}{2\tau^2}\right).$$

The posterior of τ^2 is

$$\left[\tau^2 \mid y_{ik}^{cent,c}, \mathbf{X}_{ik}, A_{ik}, V_k, b_k, \alpha_k, \sigma^2, \{\mathcal{W}_h, \mathcal{M}_h\}\right] \sim IG\left(\frac{K}{2} + 1, \frac{\sum_{k=1}^K b_k^2 + 2\alpha_k}{2\alpha_k}\right).$$

Complete derivation of the posterior distributions are also provided in Web Section S1 of Hu et al. (2022). A *single iteration* of the riAFT-BART sampling algorithm proceeds through the following steps:

1. Update b_k , τ^2 and α_k from their respective posterior distributions.
2. Using $\log y_{ik}^{cent,c} - b_k$ as the responses and $\{A_{ik}, \mathbf{X}_{ik}\}$ as the covariates, update BART sum-of-trees model via parameters μ_{lh} and σ^2 , using the Bayesian backfitting approach of Chipman et al. (Chipman et al., 2010) Directly update $f(A_{ik}, \mathbf{X}_{ik})$ using the updated BART model, for $i = 1, \dots, n_k, k = 1, \dots, K$.
3. For each $\{i, k\} \in \{i = 1, \dots, n_k, k = 1, \dots, K\}$, update z_{ik} by sampling

$$\log z_{ik} \sim \text{Truncated-Normal} \left(f(A_{ik}, \mathbf{X}_{ik}) + b_k, \sigma^2; \log y_{ik}^{cent} \right).$$

Because we use the centered responses $\log(y_{ik}^{cent}) = \log(y_{ik}) - \hat{\mu}_{AFT}$ in posterior computation, we add $\hat{\mu}_{AFT}$ back to the posterior draws of $f(A_{ik}, \mathbf{X}_{ik})$ in the final output.

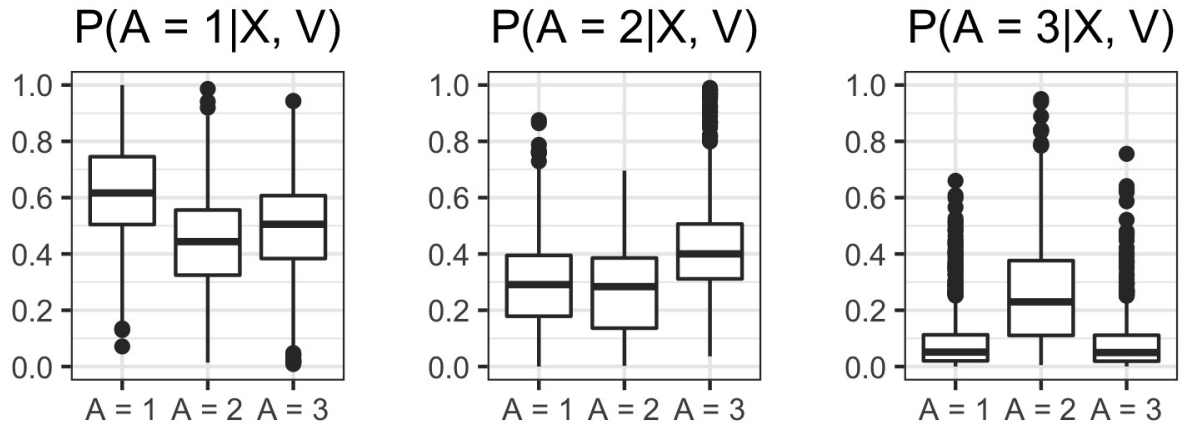
S2 Amputation details for simulation in Section 4.2

We used the multivariate amputation procedure to generate incomplete survival datasets with an overall missingness proportion of 40% in covariates. For brevity of notation, we suppress subscripts i and k . After generating the fully observed data, we amputated predictors X_5, X_6, X_7, X_8 under the missing at random mechanism using the multivariate amputation approach. We first randomly divided the full data into 8 subsamples, which were the following percentages of the whole data: 0.30, 0.09, 0.09, 0.08, 0.08, 0.16, 0.10, and 0.10. The weighted sum scores (WSS) relate the missingness on amputated variables to the values of other variables as follows:

- (1) $wss_{x_5,i} = x_3 + x_4 + x_3x_4$
- (2) $wss_{x_6,i} = x_3 + x_4 + x_5 + x_5^2 + x_3x_4$
- (3) $wss_{x_7,i} = x_4 + x_5 + x_6 + x_6^2 + x_4x_5$
- (4) $wss_{x_8,i} = x_5 + x_6 + x_7 + x_6x_7$
- (5) $wss_{x_5,x_6,i} = x_3 + x_4$
- (6) $wss_{x_6,x_7,i} = x_5$
- (7) $wss_{x_7,x_8,i} = x_4 + x_5 + 0.5x_4x_5$
- (8) $wss_{x_6,x_8,i} = x_3 + x_4 + x_3x_4$

The weighted sum score gives a nonzero weight to the variables (the right hand side of the WSS equations) and their nonlinear forms and interactions therein, on which the probabilities to be missing for amputated variables depend. The predictor variables X_5, X_6, X_7, X_8 were respectively amputated in subsample (1), subsample (2), subsample (3), and subsample (4). We further created the joint missingness in (X_5, X_6) in subsample (5), (X_6, X_7) in subsample (6), (X_7, X_8) in subsample (7) and (X_6, X_8) in subsample (8). Finally, we applied the logistic distribution function to the weighted sum scores to create the missing indicators and amputate data. A right-tailed type of missingness was used for subsamples (1)–(5) and a both-tailed type of missingness was used for subsamples (6)–(8). The amputated eight subsamples were combined to form a whole dataset. This procedure created 40% overall missingness in the covariates. The missingness proportion is 15% in X_5 , 17% in X_6 , 14% in X_7 and 11% in X_8 .

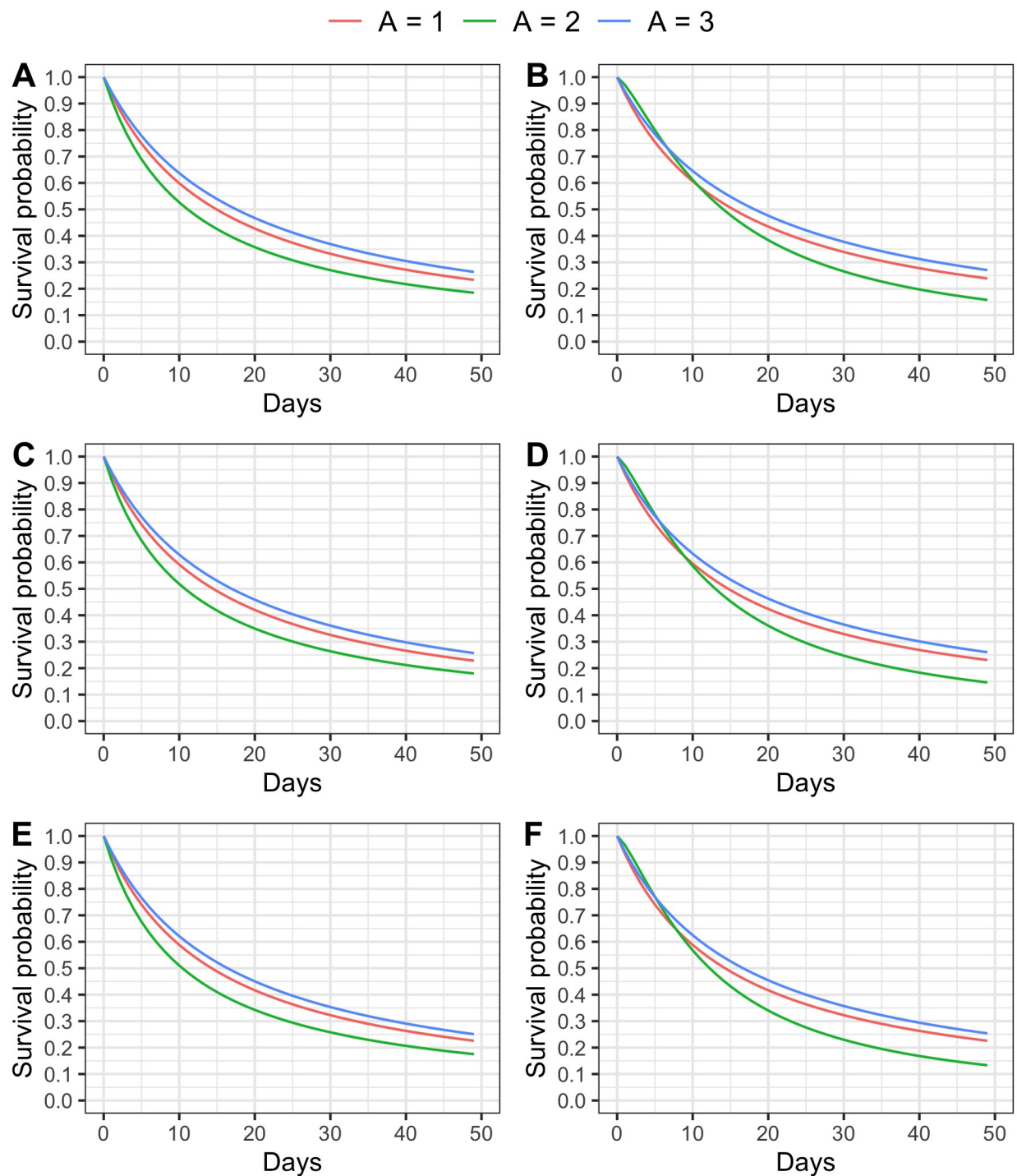
S3 Supplementary figures and tables



Web Figure 1: Overlap assessment for data simulated under moderate covariate overlap. Each panel presents boxplots by treatment group of the true generalized propensity scores for one of three treatments, and for every unit in the sample. The left panel presents treatment 1, the middle panel presents treatment 2, and the right panel presents treatment 3.

Web Table 1: Subclasses of the true generalized propensity scores (GPS) described in our simulation study in Section 4.1. The number of individuals falling in each subclass was calculated based on one data replication.

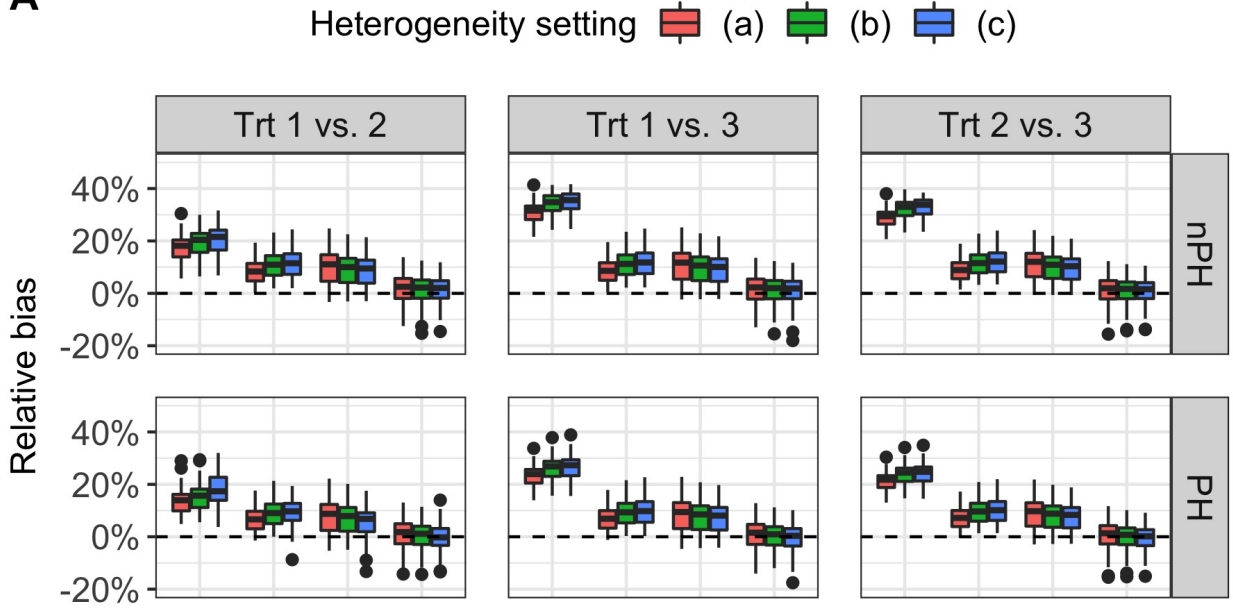
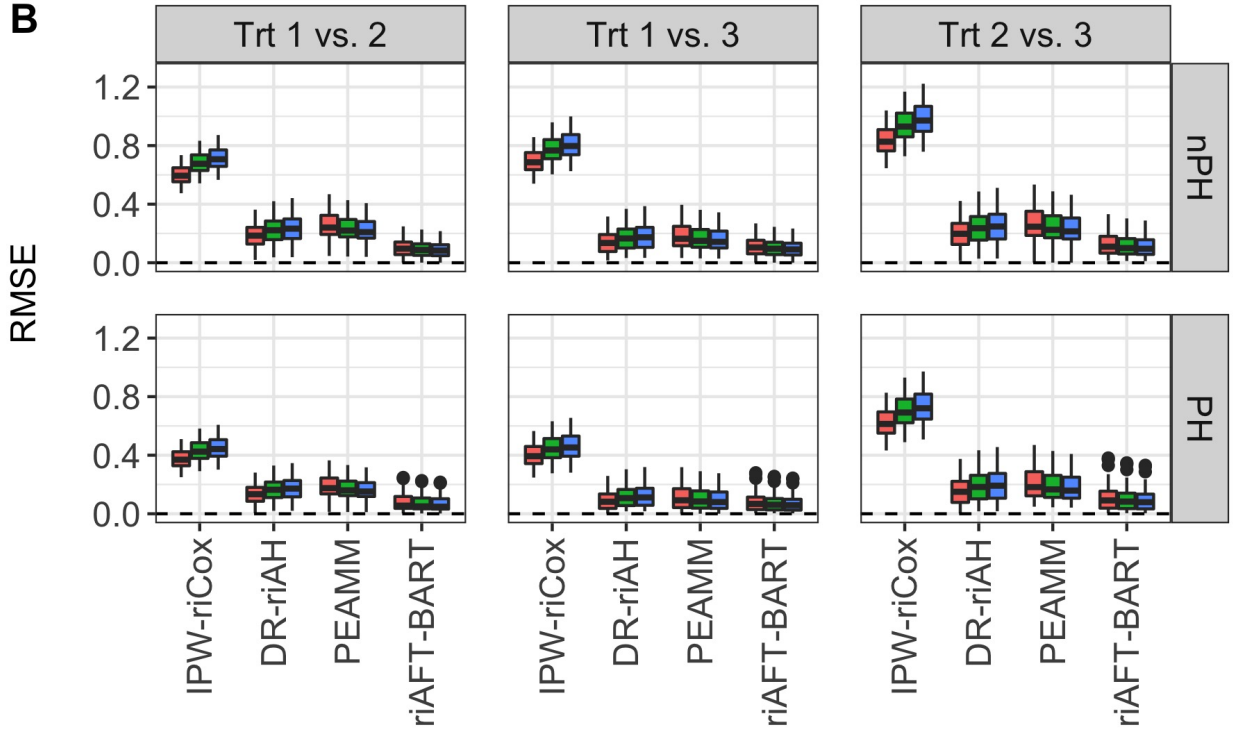
Subclass ID	GPS for treatment group 1	GPS for treatment group 2	# of individuals
1	(0, 0.1]	(0, 1]	60
2	(0, 0.2]	(0, 0.25]	52
3	(0, 0.2]	(0.25, 0.5]	48
4	(0, 0.2]	(0.5, 0.75]	52
5	(0, 0.2]	(0.75, 1]	48
6	(0.2, 0.4]	(0, 0.2]	44
7	(0.2, 0.4]	(0.2, 0.4]	45
8	(0.2, 0.4]	(0.4, 0.6]	56
9	(0.2, 0.4]	(0.6, 0.8]	42
10	(0.2, 0.4]	(0.8, 1]	41
11	(0.4, 0.5]	(0, 0.1]	42
12	(0.4, 0.5]	(0.1, 0.3]	44
13	(0.4, 0.5]	(0.3, 0.4]	46
14	(0.4, 0.5]	(0.4, 0.5]	54
15	(0.4, 0.5]	(0.5, 0.6]	56
16	(0.4, 0.5]	(0.6, 0.7]	53
17	(0.4, 0.5]	(0.7, 1]	50
18	(0.5, 0.6]	(0, 0.2]	42
19	(0.5, 0.6]	(0.2, 0.3]	44
20	(0.5, 0.6]	(0.3, 0.4]	48
21	(0.5, 0.6]	(0.4, 0.5]	56
22	(0.5, 0.6]	(0.5, 0.6]	57
23	(0.5, 0.6]	(0.6, 0.7]	46
24	(0.5, 0.6]	(0.7, 0.8]	44
25	(0.5, 0.6]	(0.8, 1]	45
26	(0.6, 0.7]	(0, 0.3]	48
27	(0.6, 0.7]	(0.3, 0.5]	45
28	(0.6, 0.7]	(0.5, 0.6]	55
29	(0.6, 0.7]	(0.6, 0.7]	52
30	(0.6, 0.7]	(0.7, 1]	50
31	(0.7, 0.8]	(0, 0.3]	45
32	(0.7, 0.8]	(0.3, 0.5]	54
33	(0.7, 0.8]	(0.5, 0.7]	52
34	(0.7, 0.8]	(0.7, 1]	46
35	(0.8, 0.9]	(0, 0.4]	57
36	(0.8, 0.9]	(0.4, 0.6]	48
37	(0.8, 0.9]	(0.6, 1]	58
38	(0.9, 1]	(0, 0.4]	63
39	(0.9, 1]	(0.4, 0.6]	52
40	(0.9, 1]	(0.6, 1]	60



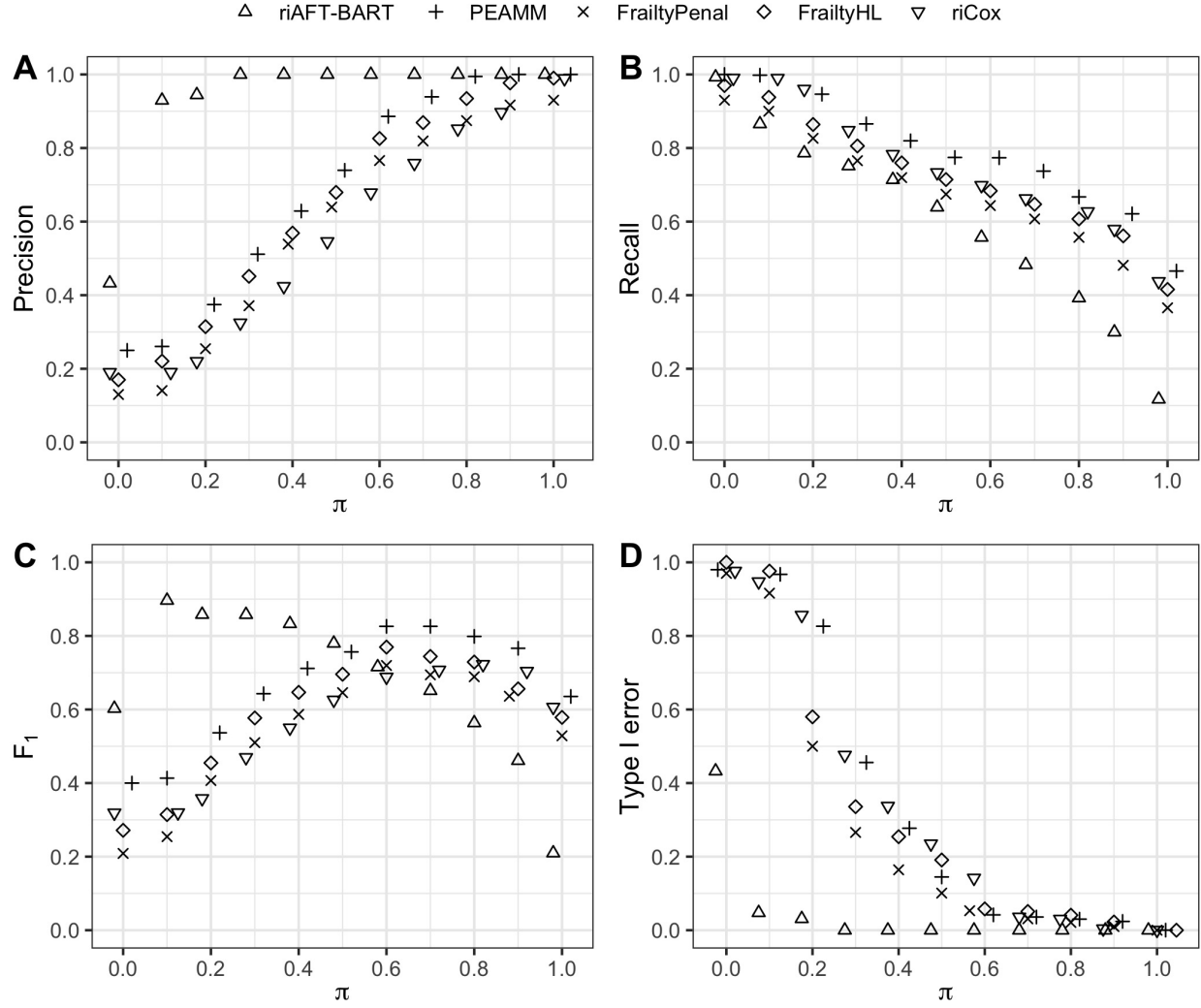
Web Figure 2: Kaplan-Meier survival curves for three treatment groups generated in our simulation study in Section 4.1. Panels A-E respectively represent scenarios corresponding to PH & HS(a), nPH & HS(a), PH & HS(b), nPH & HS(b), PH & HS(c), nPH & HS(c). PH=proportional hazards; nPH=nonproportional hazards; HS=heterogeneity setting.

Web Table 2: Mean and (standard deviation) of precision in the estimation of heterogeneity effects (PEHE) across 250 data replications for each of the 4 methods based on 3-week restricted mean survival time under six configurations: (proportional hazards (PH) vs. nonproportional hazards (nPH)) \times (heterogeneity setting (a) vs. (b) vs. (c)).

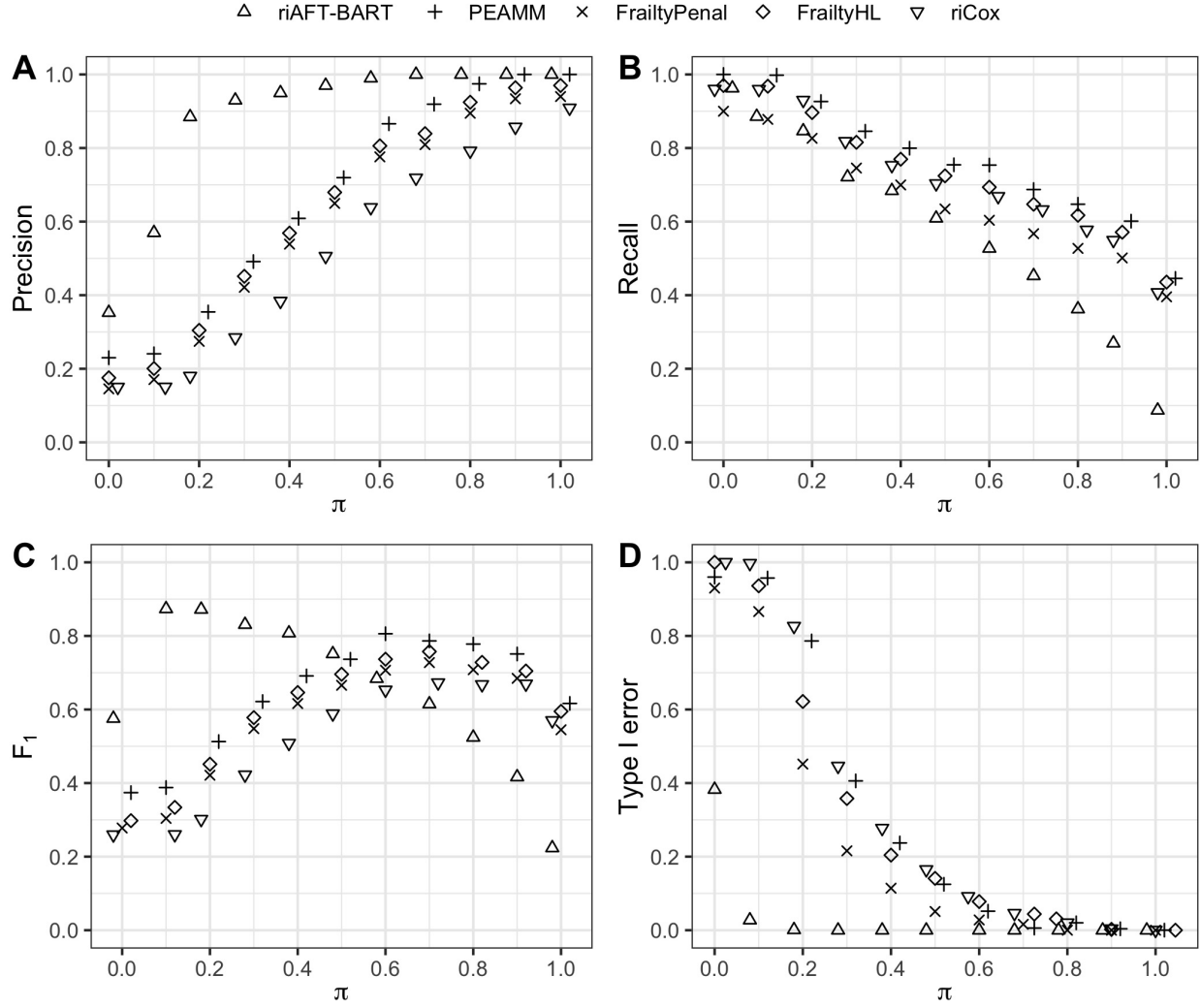
	Methods	PH			nPH		
		HS(a)	HS(b)	HS(c)	HS(a)	HS(b)	HS(c)
Trt 1 vs. 2	IPW-riCox	2.32 (.22)	2.65 (.25)	2.77 (.30)	3.12 (.27)	3.45 (.30)	3.55 (.30)
	DR-riAH	0.67 (.05)	0.75 (.05)	0.79 (.05)	0.82 (.05)	0.90 (.06)	0.94 (.06)
	PEAMM	0.89 (.06)	0.81 (.05)	0.74 (.05)	1.08 (.07)	1.00 (.06)	0.91 (.06)
	riAFT-BART	0.28 (.04)	0.24 (.03)	0.19 (.03)	0.37 (.04)	0.32 (.03)	0.27 (.03)
Trt 1 vs. 3	IPW-riCox	2.43 (.23)	2.75 (.23)	2.84 (.31)	3.23 (.28)	3.56 (.31)	3.64 (.31)
	DR-riAH	0.73 (.05)	0.76 (.05)	0.83 (.05)	0.85 (.05)	0.94 (.06)	0.99 (.06)
	PEAMM	0.93 (.06)	0.85 (.05)	0.78 (.05)	1.12 (.07)	1.02 (.06)	0.93 (.06)
	riAFT-BART	0.32 (.04)	0.27 (.03)	0.23 (.03)	0.40 (.04)	0.35 (.03)	0.30 (.03)
Trt 2 vs. 3	IPW-riCox	2.50 (.23)	2.83 (.26)	2.94 (.31)	3.30 (.28)	3.64 (.31)	3.73 (.31)
	DR-riAH	0.77 (.05)	0.84 (.05)	0.87 (.05)	0.89 (.05)	0.98 (.06)	1.01 (.06)
	PEAMM	0.97 (.06)	0.89 (.05)	0.82 (.05)	1.16 (.07)	1.06 (.06)	0.97 (.06)
	riAFT-BART	0.35 (.04)	0.30 (.03)	0.27 (.03)	0.43 (.04)	0.39 (.03)	0.35 (.03)

A**B**

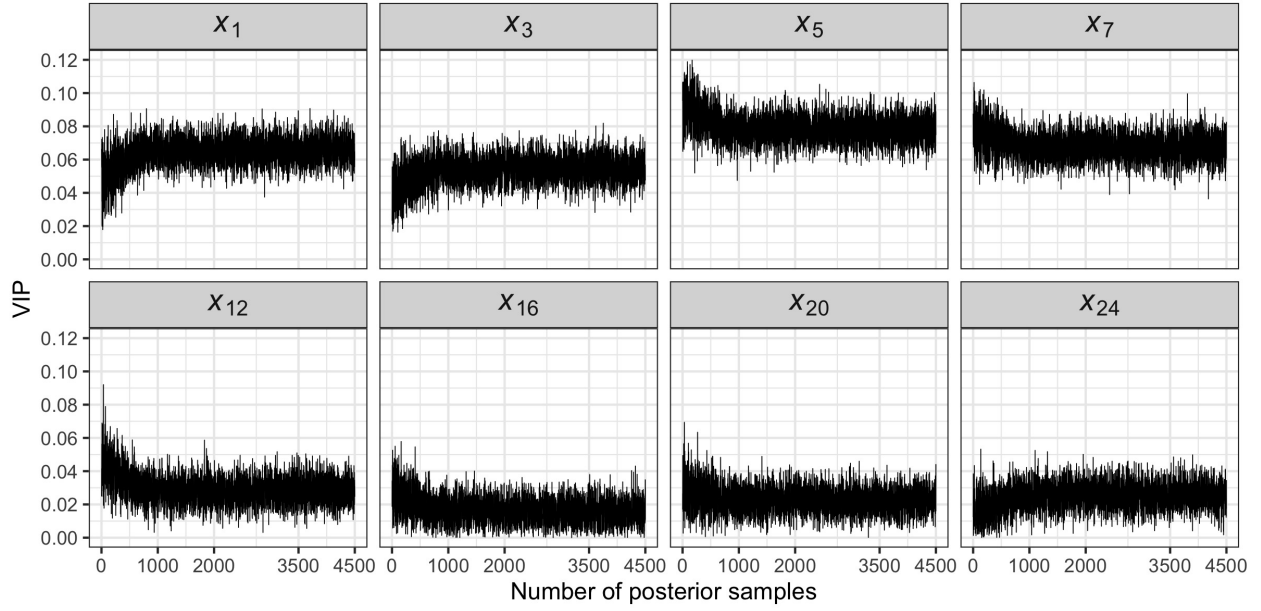
Web Figure 3: Relative biases (Panel A) and root-mean-squared-errors (RMSE) (Panel B) among 40 generalized propensity score subgroups under 6 data configurations: (heterogeneity settings a, b, c) \times (proportional hazards (PH) and nonproportional hazards (nPH)) for each of four methods, IPW-riCox, DR-riAH, PEAMM and riAFT-BART. Three pairwise treatment effects were estimated by averaging the individual survival treatment effect (based on 3-week restricted mean survival time) across individuals in each subgroup. Each boxplot visualizes the distribution of relative biases or the distribution of RMSE for 40 subgroups, each averaged across 250 simulation runs.



Web Figure 4: The precision, recall, F_1 score and Type I error, for each of four methods: riAFT-BART, PEAMM, riCox, FrailtyHL and FrailtyPenal with data generated under proportional hazards, based on 250 data replications. Imputation was performed on 100 bootstrap samples of each replication dataset, using imputation method mice. There are $K = 10$ clusters, each with a size of 200; the total sample size is 2000. The overall proportion of missingness is 40%.



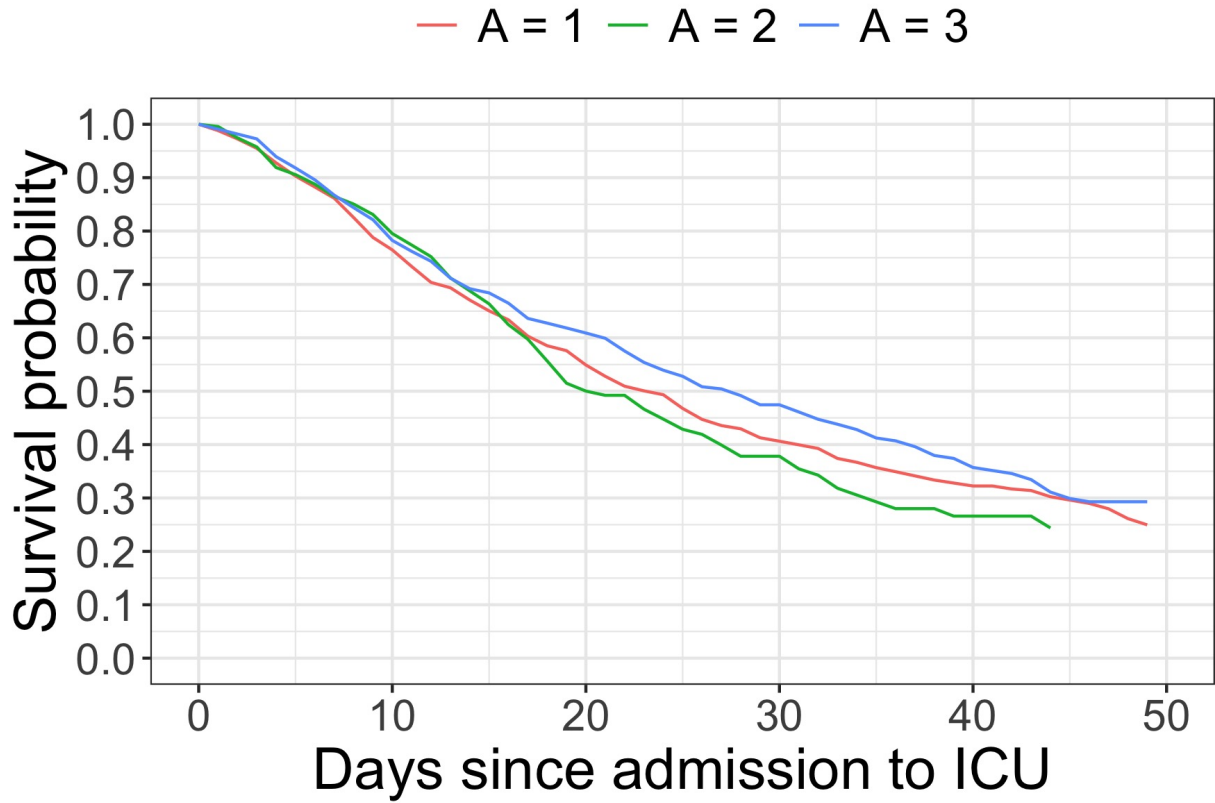
Web Figure 5: The precision, recall, F_1 score and Type I error, for each of four methods: riAFT-BART, PEAMM, riCox, FrailtyHL and FrailtyPenal with data generated under non-proportional hazards, based on 250 data replications. Imputation was performed on 100 bootstrap samples of each replication dataset, using imputation method mice. There are $K = 10$ clusters, each with a size of 200; the total sample size is 2000. The overall proportion of missingness is 40%.



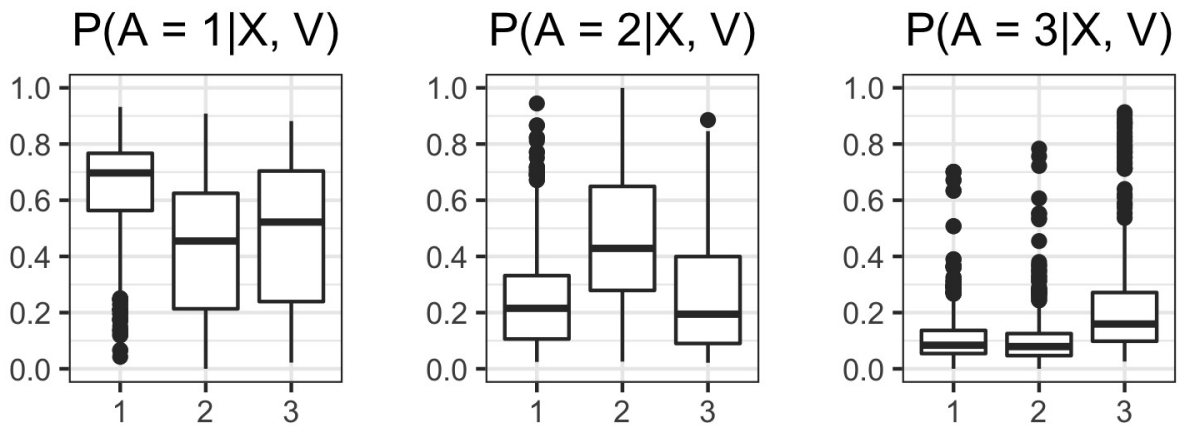
Web Figure 6: Assessing convergence of the chain by plotting 4500 posterior draws of variable selection proportions (VIP) for 4 useful predictors $X_{ik1}, X_{ik3}, X_{ik5}, X_{ik7}$ and 4 noise predictors $X_{ik12}, X_{ik16}, X_{ik20}, X_{ik24}$. The first 1000 posterior draws are discarded as burn-in.

Web Table 3: The definition of patient oxygen levels based on the use of ventilator.

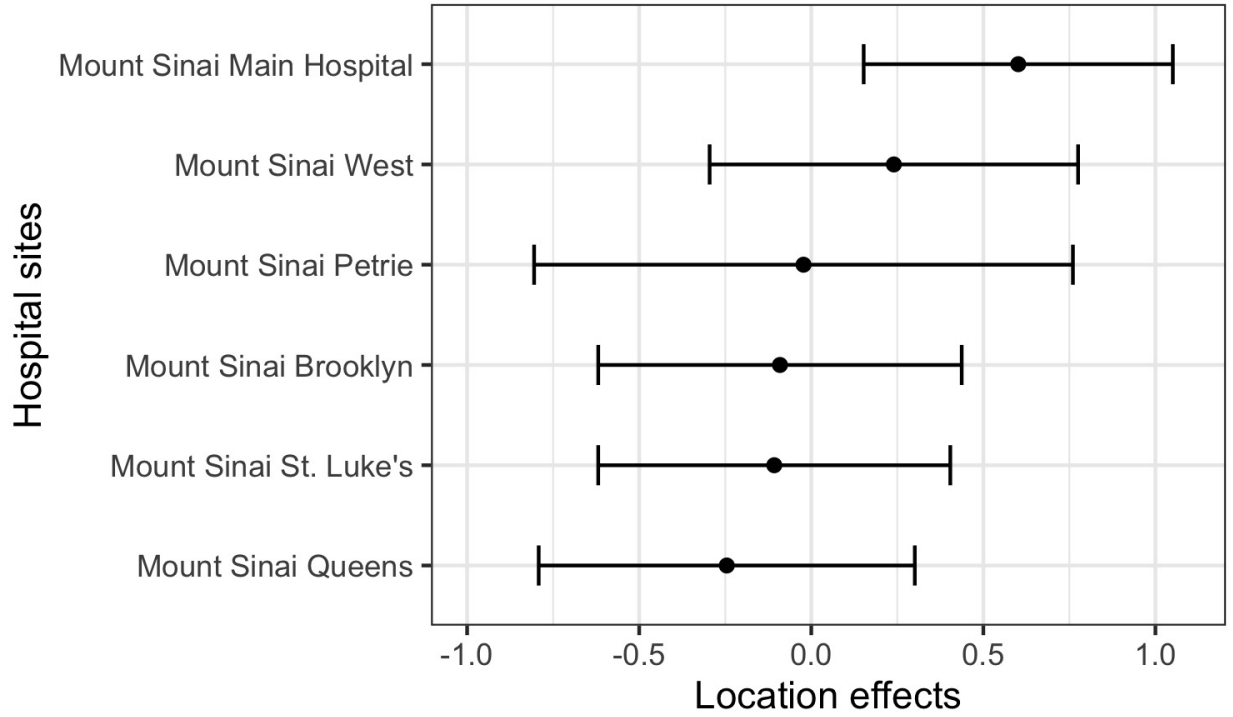
Patient oxygen level	Ventilator status
0	Room air
1	Cannula
2	Mask, Blow-by, Face tent, Oxyhood, Non-rebreather, RAM cannula
3	Continuous positive airway pressure machine, High flow nasal cannula, Hudson prongs
4	Bilevel positive airway pressure machine, Tracheostomy mask
5	Tracheotomy, Transtracheal oxygen therapy, Ventilator, Endotracheal tube, T-shaped tubing connected to an endotracheal tube, Nasal synchronized intermittent mandatory ventilation



Web Figure 7: The Kaplan-Meier survival curves for three treatment groups. Three treatment options are $A = 1$: Dexamethasone, $A = 2$: Remdesivir and $A = 3$: Dexamethasone + Remdesivir.



Web Figure 8: Overlap assessment for three treatment groups in the COVID-19 dataset. Each panel presents boxplots by treatment group of the generalized propensity scores, estimated by Super Learner, for one of three treatments, and for every individual in the sample. The left panel presents treatment 1 = Dexamethasone, the middle panel presents treatment 2 = Remdesivir, and the right panel presents treatment 3 = Dexamethasone + Remdesivir.



Web Figure 9: Examining the effect of hospital sites on patient survival in terms of the log survival days represented by the posterior mean and credible intervals of the random intercept b_k , $k = 1, \dots, 6$, for COVID-19 case study.

Web Table 5: The posterior mean and 95% credible intervals for three pairwise sample population treatment effects on patient survival for the COVID-19 case study. The effects were based on the difference in the expected log survival days. Three treatment options are $A = 1$: dexamethasone, $A = 2$: remdesivir and $A = 3$: dexamethasone + remdesivir.

$CATE_{1,2}$	$CATE_{1,3}$	$CATE_{2,3}$
0.17(-0.34, 0.68)	-0.32(-0.82, 0.18)	-0.49(-0.95, -0.03)

References

- Chipman, H. A., George, E. I., and McCulloch, R. E. (2010). BART: Bayesian additive regression trees. *The Annals of Applied Statistics* **4**, 266–298.
- Hu, L., Ji, J., Ennis, R. D., and Hogan, J. W. (2022). A flexible approach for causal inference with multiple treatments and clustered survival outcomes. *arXiv preprint* arXiv:2202.08318.